Magnetic Resonance Angiography of the Thoracic Vasculature: Technique and Applications

Daniel R. Ludwig, MD,[1] (iD) Anup S. Shetty, MD,[1] Jordi Broncano, MD,[2] (iD) Sanjeev Bhalla, MD,[1] and Constantine A. Raptis, MD[1]* (iD)

CME

Magnetic resonance angiography (MRA) is a powerful clinical tool for evaluation of the thoracic vasculature. MRA can be performed on nearly any magnetic resonance imaging (MRI) scanner, and provides images of high diagnostic quality without the use of ionizing radiation. While computed tomographic angiography (CTA) is preferred in the evaluation of hemodynamically unstable patients, MRA represents an important tool for evaluation of the thoracic vasculature in stable patients. Contrast-enhanced MRA is generally performed unless there is a specific contraindication, as it shortens the duration of the exam and provides images of higher diagnostic quality than noncontrast MRA. However, intravenous contrast is often not required to obtain a diagnostic evaluation for most clinical indications. Indeed, a variety of noncontrast MRA techniques are used for thoracic imaging, often in conjunction with contrast-enhanced MRA, each of which has a differing degree of reliance on flowing blood to produce the desired vascular signal. In this article we review contrast-enhanced MRA, with a focus on contrast agents, methods of bolus timing, and considerations in imaging acquisition. Next, we cover the mechanism of contrast, strengths, and weaknesses of various noncontrast MRA techniques. Finally, we present an approach to protocol development and review representative protocols used at our institution for a variety of thoracic applications. Further attention will be devoted to additional techniques employed to address specific clinical questions, such as delayed contrast-enhanced imaging, provocative maneuvers, electrocardiogram and respiratory gating, and phase-contrast imaging. The purpose of this article is to review basic techniques and methodology in thoracic MRA, discuss an approach to protocol development, and illustrate commonly encountered pathology on thoracic MRA examinations.
Level of Evidence: 5
Technical Efficacy Stage: 3

MAGNETIC RESONANCE ANGIOGRAPHY (MRA) has emerged as a robust clinical tool for evaluation of thoracic vascular pathology. It can be performed on nearly any magnetic resonance imaging (MRI) scanner and provides images with broad anatomic coverage, high contrast-to-noise ratio, and high diagnostic utility. Computed tomographic angiography (CTA) is also used routinely for evaluation of the thoracic vasculature. Both CTA and MRA provide similar diagnostic information, but various tradeoffs between the different modalities exist. CTA is more widely available, has a higher spatial resolution, and is acquired much more rapidly (ie, <1 minute, including the injection time). CTA is the preferred approach in an unstable patient and is more commonly performed in patients presenting to the emergency room. However, CTA requires administration of iodinated intravenous contrast, which cannot be given to patients with a contrast allergy or severe renal insufficiency.[1] Additionally, CT results in the delivery of ionizing radiation, a primary concern in pediatric and pregnant patients.[2] MRA, on the other hand, does not use ionizing radiation. Gadolinium-based contrast agents (GBCAs), while relatively contraindicated in patients with severe renal insufficiency, are not required to obtain a diagnostic evaluation for most clinical indications. However, contrast-enhanced MRA is generally performed unless there is a specific contraindication, as it shortens the duration of the exam and provides images of higher diagnostic quality. Important limitations of MRA in general include longer acquisition times (ie, >30 minutes), incompatibility with various implanted medical devices, and poor tolerability in patients with claustrophobia.

At institutions where MRI is readily available, MRA represents an important technique for evaluation of the thoracic vasculature in stable patients. However, thoracic MRA presents several challenges that are unique, or at least more pronounced in comparison to MRA outside of the thorax. Such challenges include cardiac and respiratory motion, which frequently necessitate the use of cardiac gating and either breath-holding or respiratory gating. Additionally, many noncontrast MRA techniques have poor sensitivity for in-plane flow, posing a limitation for evaluation of the great vessels of the chest, which are oriented in the transverse plane. This article reviews contrast-enhanced and noncontrast MRA techniques as applied to thoracic vascular imaging, with a focus on clinical applications of thoracic MRA, challenges unique to MRA in the thorax, and a basic approach for the development of thoracic MRA imaging protocols.

CONTRAST-ENHANCED MRA

Contrast-enhanced MRA is generally considered superior to noncontrast MRA, and has several important advantages (Table 1).[3–5] First, most contrast-enhanced MRA techniques are substantially faster than noncontrast MRA techniques (ie, single breath-hold per station), which reduces the overall time of the examination and additionally allows for imaging in multiple timepoints or phases of contrast enhancement. Second, vascular opacification is typically flow-independent, which reduces many of the flow-related artifacts seen in noncontrast MRA, and reduces the problem of overestimation of stenosis severity. Finally, contrast-enhanced MRA has a higher contrast-to-background ratio, most frequently rendering MRA images of superior diagnostic quality than noncontrast MRA, and allowing for higher quality 3D reconstructions. Disadvantages of contrast-enhanced MRA include a requirement for intravenous access, higher cost of the examination, challenges in synchronizing the contrast bolus with the imaging acquisition, and risk of adverse reaction to the contrast material. Despite these limitations, intravenous contrast is typically utilized in exams for patients who

TABLE 1. Comparison of Contrast-Enhanced MRA vs. Non-Contrast MRA

	Contrast-enhanced MRA	Noncontrast MRA
Advantages	1. Faster than noncontrast MRA techniques 2. Vascular opacification is flow independent, resulting in a higher sensitivity for detection of slow flow 3. Higher contrast-to-background ratio	1. No requirement for intravenous access 2. No exposure to GBCAs 3. Dependence on flow can be used to assess flow dynamics and flow directionality
Disadvantages	1. Requirement for intravenous access 2. Risk of allergic and physiologic reactions to GBCAs 3. Risk of nephrogenic systemic fibrosis resulting from GBCAs in patients with advanced CKD or acute kidney injury	1. Slower than contrast-enhanced MRA 2. Vascular opacification is flow dependent, resulting in flow-related artifacts and overestimation of stenosis severity 3. Lower contrast-to-background ratio

have no specific contraindication, such as a contrast allergy or severe renal impairment. GBCAs, methods of bolus timing, and contrast-enhanced MRA acquisition techniques will be discussed, with example thoracic MRA applications presented in the following sections.

Gadolinium-Based Contrast Agents

GBCAs are composed of a gadolinium ion (Gd^{3+}) coupled to a small molecular weight chelate. Gadolinium is a heavy metal that has paramagnetic properties, serving to reduce the T_1 relaxation time of blood and resulting in increased intensity on a T_1-weighted imaging sequence. Gadolinium is a member of the lanthanide family, which comprises a group of toxic heavy metals. The chelating agent serves to chaperone the gadolinium ion until it is excreted by the kidneys and, depending on the GBCA, the hepatobiliary system as well. In patients with severe renal dysfunction (ie, glomerular filtration rate [GFR] less than 30 mL/min/1.73-m^2) the increased physiologic half-life of the gadolinium chelate can result in dissociation of the gadolinium ion from its chaperone and precipitation of gadolinium-phosphate in tissues.[6] These deposited complexes can induce a fibrotic response, the presumed mechanism behind nephrogenic system fibrosis (NSF), a debilitating fibrosing condition of the skin and soft tissues.[7] NSF has been virtually eliminated since 2010, however, after initiation of routine screening for renal dysfunction prior to contrast-enhanced MRI, withholding GBCAs from patients with advanced chronic kidney disease (CKD) or acute kidney injury, and a practice shift away from using less stable GBCAs such as gadopentetate (Magnevist, Bayer, Berlin, Germany), gadodiamide (Omniscan, GE Healthcare, Milwaukee, WI), and gadoversetamide (OptiMARK, Mallinckrodt, St. Louis, MO).[6] Interestingly, several prospective studies have demonstrated that the more stable macrocyclic GCBAs may be safe for use in patients even with advanced CKD.[1,8–10] Regardless, routine screening for acute kidney injury and caution in patients with a GFR less than 30 mL/min/1.73-m^2 is recommended.

Most available GCBAs are extracellular contrast agents, meaning that they have an intravascular half-life of several minutes, and subsequently diffuse into the interstitial tissues and rapidly equilibrate between the various extracellular compartments.[11] An intravascular contrast agent, gadofosveset trisodium (Ablavar, Lantheus, N. Billerica, MA), was introduced in 2008 as a GCBA for contrast-enhanced MRA; however, it was subsequently removed from the market in 2017 due to suboptimal sales.[6] Gadofosveset, due to its high degree of reversible binding to plasma proteins such as albumin (ie, 80–90%), has an intravascular half-life of almost half an hour, and received regulatory approval for use in MRA evaluation of aortoiliac and peripheral vascular disease.[12] Gadopentate dimeglumine (MultiHance, Bracco, Princeton, NJ), despite functionally serving as an extracellular GCBA, also exhibits a mild degree of plasma protein binding, resulting in improved blood pool T_1 relaxivity compared to the other extracellular GBCAs.[13,14] Thus, in the post-gadofosveset era, gadopentate dimeglumine is the preferred agent at our institution for contrast-enhanced MRA. Gadopentate dimeglumine is administered at a dose of 0.1 mmol/kg and a rate of 2–3 mL/sec. Imaging is performed beginning at the first-pass arterial enhancement and then at multiple delayed imaging phases.

Methods of Contrast Timing

Precise timing for peak first-pass arterial enhancement can vary substantially based on the cardiac output, circulatory volume, and contrast injection rate.[15] A commonly-used approach is to perform a test injection using ~10% of the total volume and subsequently acquire low-resolution single-slice images through the region of interest in short regular intervals (eg, 1 second). The time to maximum enhancement is identified by reviewing the time series and determining the timepoint in which arterial enhancement is greatest (Fig. 1).
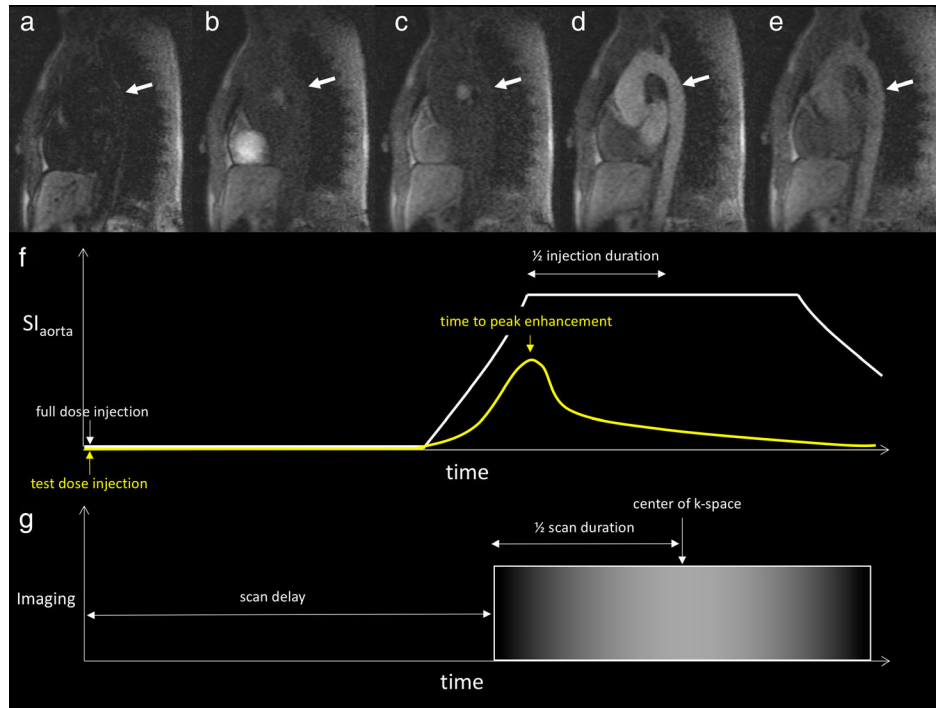
FIGURE 1: Optimization of scan delay using test dose timing examination. The patient is an 18-year-old man undergoing MRA evaluation for an ascending thoracic aortic aneurysm. Time-resolved oblique coronal MRA images after injection of 1 mL gadobenate dimeglumine (**a–e**) through the aorta (arrows) show movement of the contrast bolus through the heart, and optimal aortic opacification at 15 seconds after contrast injection (**d**). A schematic graph showing signal intensity of the aorta (SI_{aorta}) vs. time (**f**) shows an expected time–intensity curve after test dose (yellow) and full dose (white) contrast injection. Time to peak enhancement is derived empirically from the test dose injection. The duration of peak contrast enhancement is assumed to be roughly equal to the injection duration. The optimal scan delay occurs when the center of *k*-space is acquired (ie, half of the scan duration in a sequential *k*-space acquisition) during peak contrast enhancement, which is timed for the midpoint in which peak enhancement is expected to occur (ie, half of the injection duration) (**g**). Scan delay can be calculated as the time to peak enhancement, plus half of the injection duration, minus time to center of *k*-space.

The start of the acquisition is then determined according to the following formula:

$$\text{Scan delay} = (\text{injection duration}/2) + (\text{time to peak}) - (\text{time to center of } k-\text{space})$$

where scan delay represents the delay between the start of the gadolinium injection to the start of the MRA acquisition. The central portion of *k*-space determines the image contrast, and thus the acquisition of the center of *k*-space should be timed for peak arterial enhancement. In a pulse sequence that uses sequential *k*-space acquisition, time to the center of *k*-space is typically half of the acquisition duration. However, in a centric phase-encoded acquisition (ie, center of *k*-space acquired first), time to the center of *k*-space is near zero. The duration of peak arterial enhancement is assumed to be equal to the injection duration, and a delay of half the injection duration is added to the scan delay to time the center of *k*-space for the midpoint of peak enhancement.

An alternative to a test bolus technique is a best guest approximation, which uses population-based timing estimates for the time to peak parameter. For instance, time to peak from an antecubital vein to the thoracic aorta is ~15 seconds

in a younger healthy patient and 45–60 seconds in an older patient with cardiomyopathy.[13] This approach, while prone to estimation error, slightly reduces the examination time and reduces the possibility of venous contamination from the test dose injection. Yet another approach includes automated bolus detection, in which the signal intensity in a region of interest is measured continuously, and a centric acquisition is automatically triggered to begin when the signal intensity exceeds a predefined threshold. An additional technique is MR fluoroscopic triggering, in which low-resolution images of a single slice of interest are continuously acquired during and after contrast injection and displayed for the user.[16,17] When peak or near peak contrast enhancement is seen in the vessel of interest, a centric reordered MRA sequence is manually triggered. Fluoroscopic MR triggering is useful in patients with complex flow dynamics, such as those with large aneurysms in which contrast may pool before proceeding distally. While a robust technique, fluoroscopic MR triggering is less frequently used than test bolus and scan delay techniques, as it requires operator oversight, typically by a physician or highly skilled technologist. Finally, another entirely different approach is time-resolved MRA, which does not require any timing of the bolus injection. Imaging is typically started

prior to contrast injection and acquired continuously for a sufficient duration to include any necessary vascular phases. Techniques for time-resolved MRA will be discussed in further detail in a following section.

Accurate timing of the contrast bolus is critical to achieve a high-quality MRA study. If the center of *k*-space is acquired prior to peak arterial enhancement, vascular opacification will be suboptimal. Furthermore, if the center of *k*-space is acquired during a rapid change in the vascular contrast concentration (ie, upslope or downslope), ringing or banding artifact can occur and render the images nondiagnostic.[13,18] Conversely, if the acquisition is delayed and occurs after peak arterial enhancement, venous contamination can result. Although less of a problem in thoracic imaging due to the large size of the arteries of interest, venous contamination can compromise interpretation of the maximum intensity projection (MIP) images. These issues can be mitigated by performing at least one additional contrast-enhanced MRA acquisition immediately following the first acquisition timed for peak first-pass arterial enhancement.[15]

3D Spoiled Gradient Echo

3D spoiled gradient recalled echo (GRE) sequences (ie, fast low angle shot [FLASH], spoiled gradient recalled acquisition [SPGR], T_1-fast field echo [T_1-FFE]) are most commonly used for contrast-enhanced MRA. Key strengths of 3D spoiled GRE include strong inherent T_1-weighting, rapid acquisition speeds, high spatial resolution, high signal-to-noise ratio (SNR), and robust background suppression.[19,20] Echo time (TE) and relaxation time (TR) are minimized (<3 msec and <5 msec, respectively) to speed acquisition time and preserve T_1-weighting.[3] A combination of radiofrequency (RF) spoiling, inversion recovery, fat suppression, and subtractive techniques are used for background suppression.[21] Flip angles typically range from 25–40°, where a higher flip angle results in further background suppression, but may slightly attenuate the gadolinium signal. Ideally, the acquisition is optimized so that the entire sequence can be obtained in a single breath-hold (typically less than 20 seconds). An isotropic acquisition is preferred to allow for distortion-free multiplanar reformats (MPR) images, but is typically not possible to allow for acceptable sequence times. Thus, most MRA applications are anisotropic, with in-plane resolution maximized while through-plane resolution decreased, allowing for greater anatomic coverage in an acceptable amount of time. Contrast-enhanced MRA using a 3D spoiled GRE acquisition produces high-resolution angiographic images with excellent background suppression that are optimized for intraluminal vascular evaluation (Fig. 2).

Typically, 3D GRE image sets used in MRA are obtained with the breath-holding technique, but not electrocardiogram (ECG) or respiratory gating. This is typically sufficient for generating image sets that are adequate for
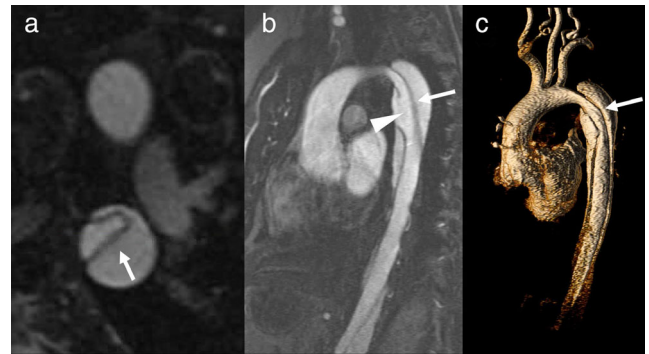

FIGURE 2: Contrast-enhanced MRA of a Type B aortic dissection in a 38-year-old woman with Marfan syndrome presenting with back pain. Transaxial (a) and oblique coronal (b) contrast-enhanced MRA images demonstrate an intimomedial dissection flap within the descending thoracic aorta (arrows), in keeping with Type B dissection. A large fenestration is noted between the true and false lumen in the proximal descending thoracic aorta (arrowhead). Volume-rendered MRA image (c) again shows the Type B dissection, with the false lumen wrapping around the true lumen (arrow). The patient was managed conservatively with strict blood pressure and heart rate control and discharged in stable condition.

evaluating the major vessels of the thorax. Given a typical 10–20-second acquisition for the 3D GRE sequences used in MRA, vessels or structures that are moving may be degraded by motion. One important example in thoracic MRA is motion at the level of the aortic root, which may complicate size measurements of the valve plane, sinuses of Valsalva, and sinotubular junction. ECG and respiratory gating, when employed, may reduce or eliminate motion at the aortic root (Fig. 3).[22,23] Given that time constraints for breath-holding are irrelevant during a respiratory-gated acquisition, isotropic voxels can be used, which allow for distortion-free MPR images. Of note, when imaging the larger vessels of the thorax, respiratory gated sequences can use a relatively wide acceptance window of 3–5 mm, which will decrease scan time.[24] As respiratory and ECG gated sequence can take upwards of 5 minutes, it is important to instruct the patient to remain still and breathe as evenly as possible. If the patient moves during the exam, motion artifact will be distributed throughout the dataset and will not be recognized until the entire volume of images have been acquired.

The volume-interpolated GRE (ie, volumetric interpolated breath-hold examination [VIBE], liver acquisition with volume acceleration [LAVA], T_1-weighted high resolution isotropic volume examination [THRIVE], T_1-weighted gradient echo [TIGRE]) represents a variation of the 3D spoiled GRE sequence that is used to increase background signal for better evaluation of background tissues, and is accomplished by decreasing the flip angle to 10–15° and using a symmetric readout in the k_y direction.[13,25] Indeed, the volume-interpolated GRE is used in almost all contrast-enhanced body MRI protocols for depiction of background anatomy and parenchymal enhancement. Volume-interpolated GRE is
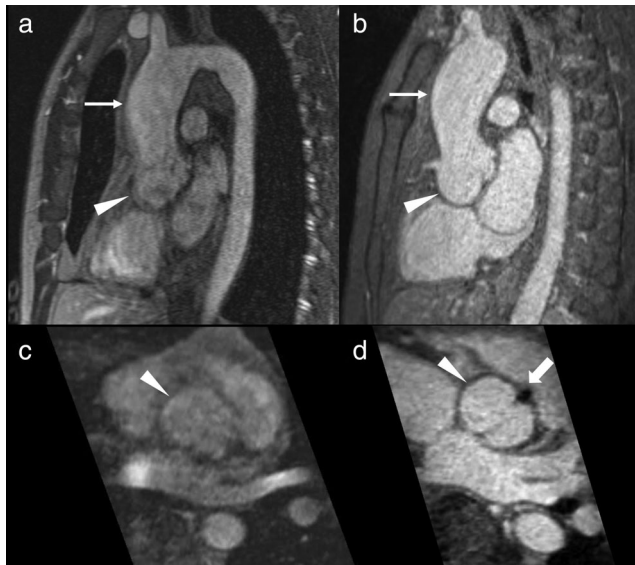
FIGURE 3: ECG and respiratory gated contrast-enhanced MRA of a right coronary sinus aneurysm in a 47-year-old man with bicuspid aortic valve and ascending aortopathy. Oblique coronal contrast-enhanced MRA images in the arterial phase during a breath-hold (a) and using ECG and respiratory gating with isotropic voxels (b) shows an ascending aortic aneurysm (thin arrows) and asymmetric enlargement of the right coronary sinus (arrowheads). Corresponding axial MPR images through the aortic root (c and d, corresponding to reformatted images from a and b, respectively) show the enlarged right coronary sinus to better advantage (arrowheads). Pulsation artifact involving the aortic root is substantially improved using ECG and respiratory gating (b and d vs. a and c). As the time constraints for breath-holding are not relevant during a respiratory-gated acquisition, isotropic voxels can be obtained which allow for distortion-free MPR images (d). Bicuspid valve morphology with associated valvular calcification (thick arrow) is only appreciated on the ECG and respiratory gated image (d).

also useful in the MR angiography setting for evaluation of the vascular wall, specifically when vasculitis or perivasculitis is suspected (Fig. 4). Volume-interpolated GRE also provides excellent intraluminal opacification, and performs well in the evaluation for pulmonary embolism (Fig. 5). In patients with limited ability to cooperate with breath-holding instruction, the volume-interpreted GRE sequence can be acquired using a radial *k*-space (rather than Cartesian) technique (ie, StarVIBE, BLADE, periodically rotated overlapping paralel lines with enhanced reconstruction [PROPELLER]), which reduces the conspicuity of motion artifacts due to its lack of unique frequency- and phase-encoded directions.[26]

Time-Resolved MRA

In time-resolved MRA, imaging is typically started prior to contrast injection and acquired continuously, as discussed above. The acquisition is optimized to maximize temporal resolution with a temporal resolution of 8 seconds or better, ensuring at least one adequate arterial phase will be obtained. Typical sequence modification includes reducing anatomic coverage, decreasing spatial resolution, reducing the repetition
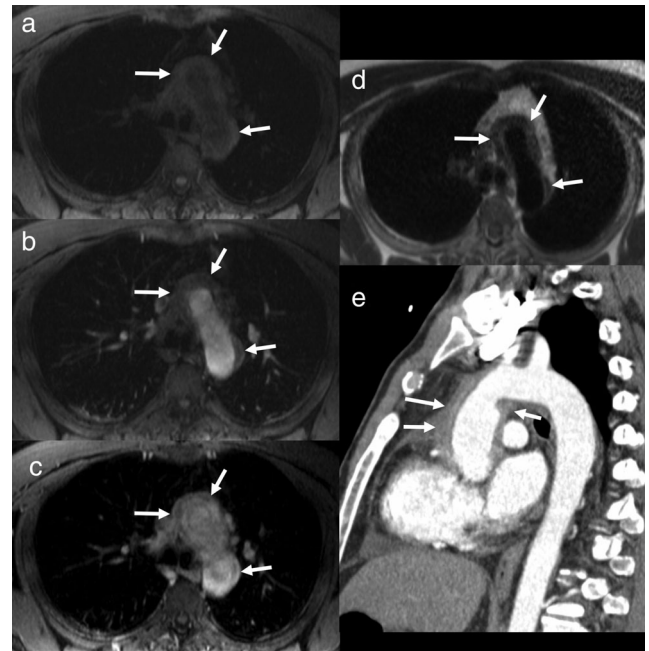
FIGURE 4: Volume-interpolated GRE and delayed imaging of periaortitis in a 42-year-old man presenting with chest pain. Precontrast volume-interpolated GRE (a), postcontrast volume-interpolated GRE after a 90-second delay (b), and postcontrast volume-interpolated GRE obtained after a 5-minute delay (c) show a circumferential rind of soft tissue surrounding the aortic arch (arrows), which demonstrates progressive contrast enhancement most pronounced after a 5-minute delay. Corresponding transaxial T_2-weighted black-blood single-shot FSE MR image (d) show intermediate signal intensity soft tissue surrounding the aorta (arrows) rather than within the aortic wall, suggestive of periaortitis rather than vasculitis. Contemporaneous oblique coronal CT image (e) demonstrates the extent of periaortic involvement (arrows), which included the ascending aorta and aortic arch. Immunologic workup was positive only for elevated inflammatory markers, and the patient was initiated on mycophenolate mofetil.
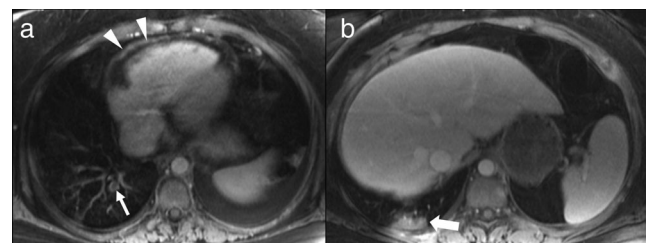
FIGURE 5: Volume-interpolated GRE imaging of incidental pulmonary embolism and pulmonary infarction in a 34-year-old woman undergoing evaluation for a mass in the superior mediastinum. Postcontrast transaxial volume-interpolated GRE images (a,b, respectively) show a filling defect in the posterior basal segmental artery of the right lower lobe (thin arrow), consistent with pulmonary embolism. There is an associated infarct within the posterior basal segment of the right lower lobe (thick arrow). Note is also made of nodular enhancing soft tissue involving the parietal pericardium (arrowhead), presumably malignant in etiology. Biopsy of the superior mediastinal soft tissue (not shown) demonstrated poorly differentiated adenocarcinoma of unknown primary. She was initiated on therapeutic anticoagulation and managed with systemic chemotherapy and palliative radiation to the chest.
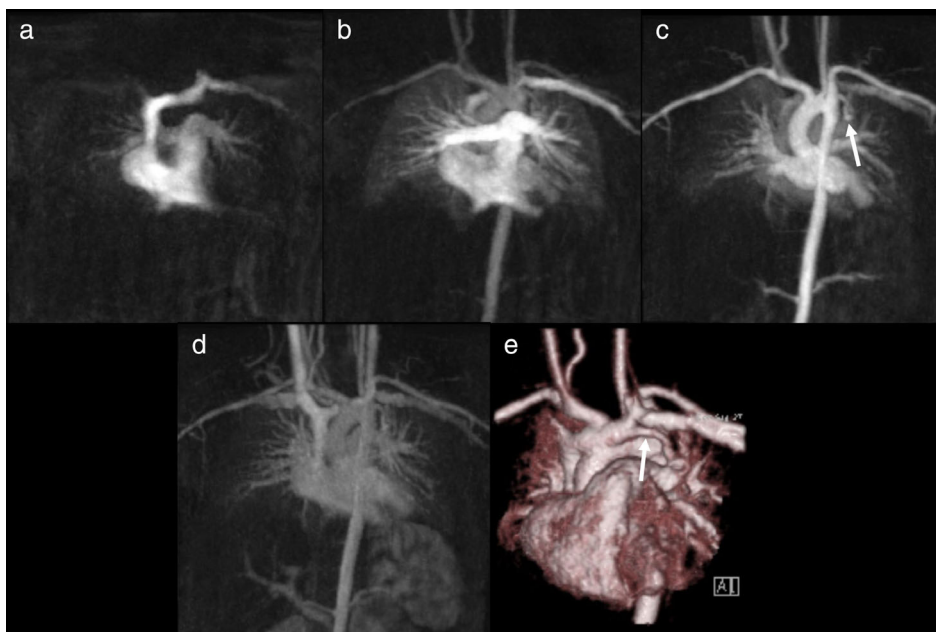
FIGURE 6: Sequential time-resolved MRA of partial anomalous pulmonary venous return (PAPVR) in a 9-year-old girl with Turner syndrome. Sequential time-resolved MRA MIP images in the coronal plane (a–d) show transit of contrast through the right heart, pulmonary arteries, pulmonary veins, left heart, and aorta. There is a left upper lobe PAPVR that drains into the left brachiocephalic vein (arrow). 3D volume-rendered images show the left upper lobe PAPVR (arrow) to better advantage (e). Due to its small size, the left upper lobe PAPVR was managed conservatively.

time, utilizing parallel imaging or partial Fourier sampling, and employing compressed sensing approaches.[13,27–29] A variety of techniques have been developed to even further improve temporal resolution in time-resolved MRA, and are largely reliant on an approach known as k-space sharing.[30] The data center of k-space space contributes mainly to image contrast, whereas data in the periphery of k-space contributes mainly to edge detail. Thus, k-space sharing fundamentally entails acquiring only portions of k-space with oversampling of the center of k-space at each acquisition timepoint, and reconstructing time-resolved image data by sharing data between timepoints. Image contrast changes rapidly as the contrast bolus is administered, whereas edge detail remains relatively fixed, so the periphery of k-space typically can be undersampled. For example, in 4D time-resolved angiography using keyhole (4D-TRAK), the center ellipsoid (ie, a keyhole) of k-space is sampled at each timepoint, whereas the periphery of k-space is sampled only at the last timepoint and the data shared to reconstruct each timepoint.[31] Other vendor-specific implementations of k-space sharing techniques include time-resolved imaging of contrast kinetics (TRICKS) and time-resolved angiography with stochastic trajectories (TWIST). K-space sharing techniques can increase the temporal resolution to less than a second, often as low as 200–300 msec, allowing for precise depiction of directionality of flow and contrast kinetics.

Time-resolved MRA is used most frequently for detailed assessment of peripheral vascular malformations.[32] However, its use in the thorax is increasing, in particular for assessment of the pulmonary vasculature such as anomalous pulmonary venous return (Fig. 6) and chronic thromboembolic pulmonary hypertension,[33,34] as well as in assessment of the central veins. Time-resolved MRA may also aid in the identification of pulmonary parenchymal perfusion defects in patients with acute or chronic pulmonary embolism.[33]

Postprocessing Techniques

Postprocessing is an important tool to facilitate interpretation of contrast-enhanced MRA data, and is especially important when techniques such as time-resolved MRA are performed, which typically generate thousands of source images. Subtraction is used routinely in contrast-enhanced MRA to optimize background suppression. The unenhanced MRA acquisition (ie, mask) is subtracted from the contrast-enhanced MRA acquisition, and the resulting images show only enhancement of the vessels and enhancing organs, provided there is no motion between the two acquisitions and the breath-holds are reproducible. MPR, another postprocessing technique described above, involves the reconstruction of image data in any plane of interest. MPR images are mandatory to generate reproducible short-axis measurements in a true perpendicular plane to the vessel course.[35] Another commonly used postprocessing tool is MIP reconstructions, which involve the generation of images that display image data in a specified projection, with the brightest voxel along each ray perpendicular to the
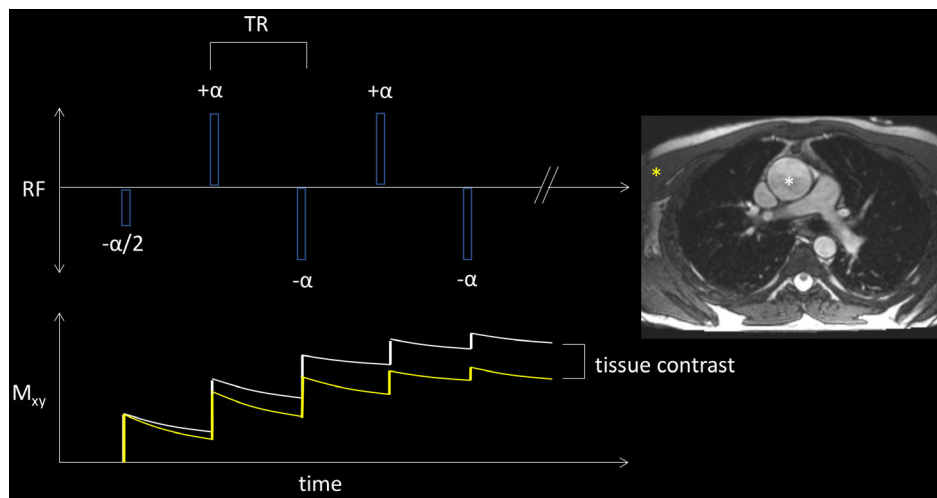
FIGURE 7: Mechanism of contrast in bSSFP imaging. A series of equally spaced RF pulses are applied with TR substantially shorter than T_2, which serves to preserve the residual transverse magnetization (M_{xy}). The result is an image with T_2/T_1 weighting, in which the blood pool is bright (white asterisk) and muscle has a dark signal intensity (yellow asterisk).

viewing plane retained (Fig. 6). MIP images are particularly useful when background suppression is optimized and there is little to no venous contamination.[13] As with all postprocessing techniques, but with MIP postprocessing in particular, all findings should be confirmed on the source dataset to ensure the finding is not related to a postprocessing artifact. Finally, volume rendering represents a less commonly used postprocessing technique in MRA, in which all voxels in the dataset are used to generate a 3D representation, most useful for representation of a specific finding to a clinician less familiar with MRA (Fig. 6). In contradiction to MIP images, in which only the maximum value along the ray is maintained, in volume rendering each voxel is assigned an opacity between 0–100% and retained in the volumetric representation.

NONCONTRAST MRA

A variety of noncontrast MRA techniques are used for thoracic imaging. Many of these techniques are used in conjunction with contrast-enhanced MRA, as noncontrast MRA often provides enhanced visualization of the background static anatomy and vessel wall, while contrast-enhanced MRA often emphasizes the lumen. Most of these methods produce images with a bright signal intensity within vascular structures (ie, bright-blood imaging). However, several approaches produce images with low signal intensity within the vasculature (ie, dark-blood imaging) and are thus optimized for detecting mural vascular and extraluminal pathology. Each technique has differing degrees of reliance on flowing blood to produce the desired vascular signal. The mechanism of contrast, advantages, and disadvantages of these noncontrast techniques with example thoracic applications will be discussed in the following sections.

Balanced Steady-State Free Precession

Balanced steady-state free precession (bSSFP) MRI (ie, true fast imaging with steady-state precession [TrueFISP], fast imaging employing steady-state acquisition [FIESTA], balanced-fast field echo [Balanced-FFE]) is a workhorse technique for cardiac imaging, and has numerous applications for the thoracic vasculature.[36] bSSFP is a noncontrast brightblood imaging technique in which the bright signal intensity in the vasculature is dependent solely on the fluid nature of the blood pool, and thus has minimal to no reliance on blood flow.[37] bSSFP imaging is performed by applying a series of equally spaced RF pulses, consisting of an initial $-\alpha/2$ pulse, and subsequent $+\alpha$ and $-\alpha$ RF pulses with alternating signs, which serve to maintain both the longitudinal and transverse magnetization in a steady state (Fig. 7).[38] The signal intensity of the resultant image is proportional to the ratio of T_2/T_1. Imaging gradients must be balanced in all directions to ensure equal dephasing and rephasing and to avoid resonant offset artifacts.[39] The TR is typically less than 5 msec, to minimize signal loss related to dephasing of transverse magnetization in regions of magnetic field inhomogeneity.[21] Thus, bSSFP sequences can be performed quickly and are suitable for retrospectively ECG-gated cine imaging.[15] Fat suppression may be used to suppress the background signal since fat, like blood, has a high T_2/T_1 ratio. bSSFP imaging is aptly suited to imaging slow flow, owing to the intrinsically bright signal of the blood pool.

bSSFP imaging is a versatile technique with several important applications that are widely incorporated into thoracic vascular imaging protocols. Using a single-shot technique and prospective ECG gating, an entire stack of bSSFP images can be obtained in a single breath-hold. When performed at the onset of an examination, bSSFP sequences are well suited to aid in the assessment of imaging coverage and
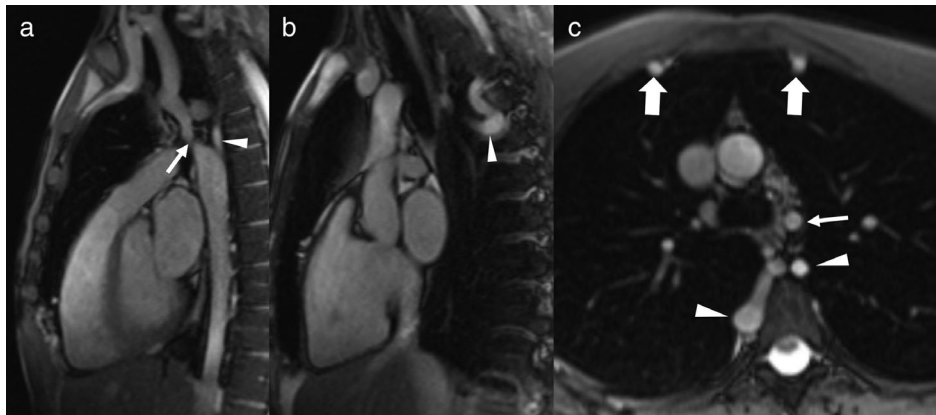
FIGURE 8: bSSFP MRI of aortic coarctation in a 20-year-old man. Sequential oblique sagittal single-shot bSSFP MR images (**a,b**) demonstrate severe narrowing at the level of the aortic isthmus (thin arrow), consistent with aortic coarctation. There are multiple enlarged intercostal arteries (arrowheads), providing collateral flow to the descending aorta. Transaxial single-shot bSSFP MR image (**c**) also shows enlargement of the internal mammary arteries (thick arrows). The patient subsequently underwent surgical repair with an interposition graft.

localize lesions of interest. bSSFP sequences are ideal for non-contrast evaluation of the luminal aorta (Fig. 8) and readily depict the presence of a dissection flap (Fig. 9).[40] A retrospectively ECG-gated single-plane bSSFP cine acquisition can be performed for evaluation of the aortic valve and aortic flow dynamics (Fig. 10). High-resolution bSSFP imaging using isotropic voxels (ie, equal dimensions of a voxel in all three planes) with ECG and respiratory gating can be employed for imaging volumes that are optimized for creating MPR and obtaining precise double-oblique measurements.[41–44] In this setting, ECG gating is performed prospectively, with k-space acquisition in diastole to minimize pulsation artifacts. Respiratory gating is performed by limiting the acquisition to only a portion of the respiratory cycle, typically end-expiration. Generally, this is performed using a respiratory-navigated sequence, in which the diaphragm is imaged continuously and k-space data are acquired with the diaphragm within a prespecified acceptance window.[24] Additional considerations for respiratory gating are discussed in further detail below.

An important limitation of bSSFP imaging is sensitivity to magnetic field inhomogeneity, and thus higher signal loss related to implantable devices such as pacemakers or replacement valves.[45,46] Similarly, bSSFP images commonly harbor Moire fringe artifacts at the edges of the field-of-view due to spatial magnetic field inhomogeneity. Additionally, owing to the out-of-phase short TE used in bSSFP sequences (ie, <2 msec), bSSFP images demonstrate India ink artifact, which may limit the identification of mural and cardiac thrombi due to signal loss at the wall of vascular structures.[15,47]

Time-of-Flight

Time-of-flight (TOF) is a commonly used bright-blood non-contrast MRA imaging technique.[36,48] In contradistinction to bSSFP MRI, TOF signal has a high reliance on inflowing blood.[49] Imaging is performed after saturation of the imaging section using repeated excitation pulses; flowing blood enters the imaging plane with unsaturated spins, resulting in bright-blood signal and robust background suppression (Fig. 11). Flow compensation gradients and techniques to minimize TE such as a fractional echo readout serve to reduce flow-related dephasing.[15,50,51] Additionally, saturation bands can be
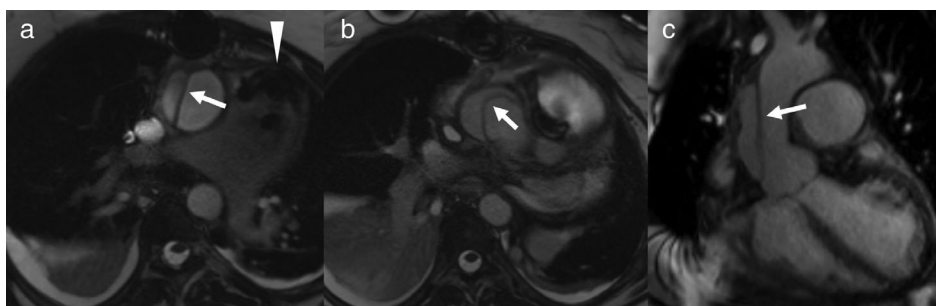
FIGURE 9: bSSFP MRI of aortic dissection in a 54-year-old woman shortly after pulmonic valve replacement for pulmonic insufficiency related to congenital rubella. Sequential single-shot bSSFP MR images (**a,b**, respectively) demonstrate a dissection flap within the ascending aorta which extends into the aortic root (arrows), in keeping with Type A dissection. Oblique coronal single-shot bSSFP MR image (**c**) demonstrates the extent of the dissection (arrow). Note the signal loss at the pulmonic valve related to the prosthesis (arrowhead). She was treated surgically with ascending aortic graft repair.
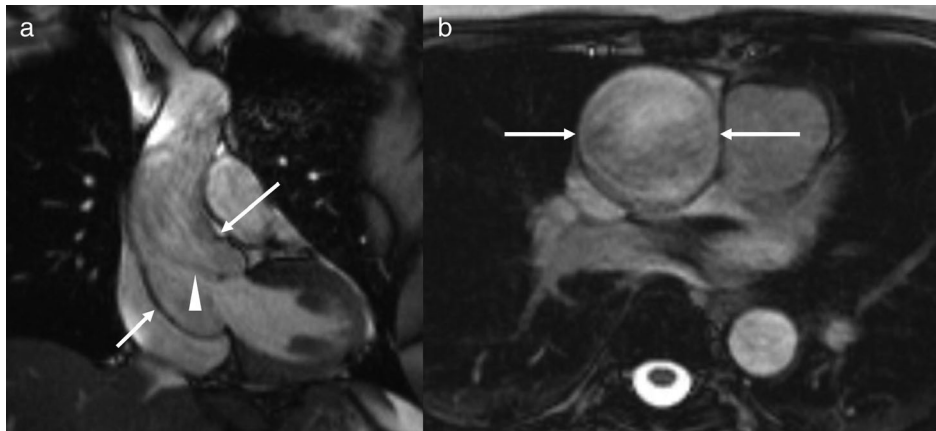
FIGURE 10: Cine bSSFP MRI of bicuspid aortopathy in a 56-year-old woman. Oblique coronal cine bSSFP (a) and transaxial bSSFP single-shot (b) MR images demonstrate an ascending thoracic aortic aneurysm measuring up to 5 cm, with effacement of the sinotubular junction (arrows). There is aortic stenosis, as evidenced by a mild stenotic flow jet (arrowhead), in keeping with bicuspid aortic valve and associated aortopathy. She did not undergo surgical repair at the time of imaging, and subsequently presented acutely 10 months later with a ruptured Type A aortic dissection requiring emergent surgical repair.

applied above or below the imaging section to null inflowing blood from either veins or arteries, resulting in purely arterial or venous signal. For instance, a saturation band placed inferiorly during TOF MRA of the thorax results in nulling venous inflow from the inferior vena cava. Thinner slices and a longer TR increase the sensitivity of TOF for detection of slow flow, as fresh unsaturated blood has a shorter distance and more time to travel into the imaging section.[15] Notably, TOF is more resistant to motion than subtractive techniques, which rely on coregistration between two separate acquisitions, such as pre- and postcontrast. While TOF is used in many noncontrast MRA protocols in the head and neck, as well as the abdominal aorta and peripheral vasculature, its use in the thorax is more limited. TOF can be useful in the noncontrast assessment of the great vessels of the chest and neck (Fig. 12), as well as for noncontrast imaging of the vasculature at the thoracic outlet (Fig. 13).[52]

The most important limitation of TOF is its sensitivity for only through-plane flow. In-plane flow results in the inflow of saturated blood and poor vascular signal, which can mimic thrombus or occlusion.[53] Furthermore, reversal in the expected direction of flow within a vessel can mimic occlusion when a saturation band is placed to null inflowing blood (Fig. 12). This phenomenon, however, can be leveraged to determine the direction of flow, using separate acquisitions with saturation bands above and below the imaging section of interest. For example, this technique can be used to determine vertebral artery flow direction in the setting of suspected
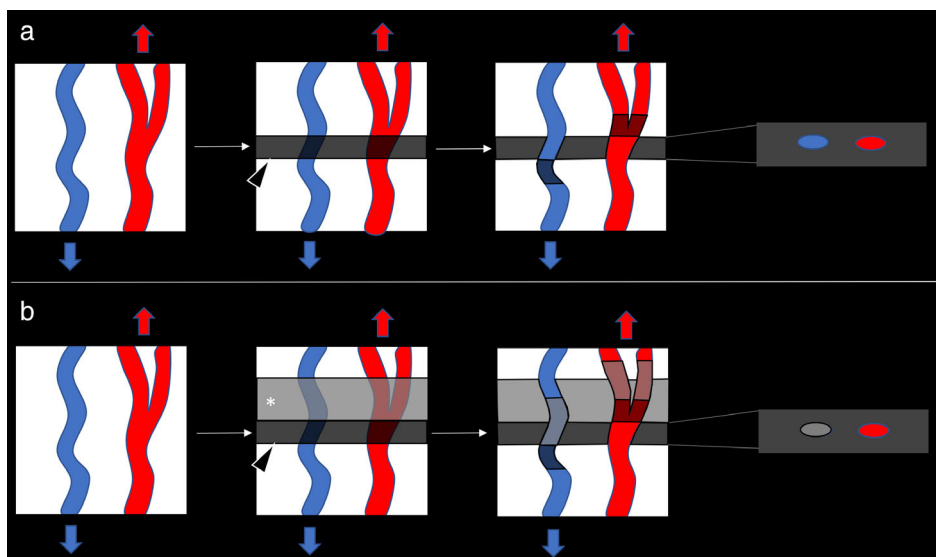
FIGURE 11: Mechanism of contrast in TOF angiography. In routine TOF imaging (a), saturation of the imaging section is performed using repeated excited pulses (arrowhead). After a time interval equivalent to TR, flowing unsaturated arterial and venous blood has time to enter the imaging plane, producing a bright signal on the TOF image. If a saturation band is applied above the imaging section to null inflowing venous blood (asterisk), only the inflowing arterial blood produces a bright signal on the TOF MRA image (b).

FIGURE 12: TOF MRA of subclavian steal phenomenon in a 32-year-old man with Takayasu's arteritis. Sequential transaxial TOF angiographic MR images obtained with a superior saturation band to suppress venous signal (a,b) demonstrate a lack of anterograde flow in the left subclavian artery (arrowhead) and left vertebral artery (thin arrow). These findings are seen to better advantage on a coronal MIP (c). Subsequent coronal MIP contrast-enhanced MRA image (d) demonstrates occlusion of the proximal left subclavian artery (arrowhead), with opacification of the left vertebral artery (thin arrow) and left subclavian artery distal to the takeoff of the left vertebral artery (thick arrow). These findings are consistent with retrograde flow in the left vertebral artery, which provides flow to the left subclavian artery (ie, subclavian steal phenomenon). The patient was treated with left carotid to subclavian artery bypass grafting and eventually required endovascular repair of his thoracoabdominal aorta after he developed multiple aortic pseudoaneurysms.

subclavian steal. TOF MRA is most commonly performed as a 2D technique; however, 3D TOF allows for high-resolution isotropic imaging, at the cost of increased blood saturation from in-slab flow, and its use is limited mainly to the brain. Additionally, TOF is further limited by long acquisition times and can overestimate the degree of stenosis owing to spin dephasing related to turbulent flow.[13]

Quiescent Interval Single Shot

Quiescent interval single shot (QISS) is a relatively new non-contrast MRA technique, which is conceptually similar to TOF MRA, and similarly has a high reliance on flowing blood due to its reliance on inflow-related enhancement.[54,55] However, unlike TOF, QISS MRA is performed using cardiac ECG-gated bSSFP sequences and a single-shot technique.[53] Briefly, the section of interest is saturated shortly after the R-wave (ie, 100 msec delay). A second saturation pulse is applied above or below the imaging section to null venous inflow. Imaging occurs in diastole, when arterial flow is minimal or slow, after a quiescent interval of 200–300 msec using a single-shot bSSFP technique, and thus a 2D slice is acquired in a single heartbeat (Fig. 14). QISS has several advantages over conventional TOF. First, the quiescent interval is much longer than the TR used in TOF imaging (ie, 30 msec), allowing for a greater time for arterial inflow and thus a higher sensitivity for slowly flowing blood, down to as low as 10 cm/s.[13] Accordingly, QISS MRA is less likely than TOF to overestimate the degree of a stenosis. Second, QISS can be performed much more rapidly than conventional TOF due to the single-shot nature of the acquisition. The entire thorax can be imaged in under a minute using QISS in several sequential breath-holds, compared to 5–10 minutes using TOF. Finally, owing to diastolic
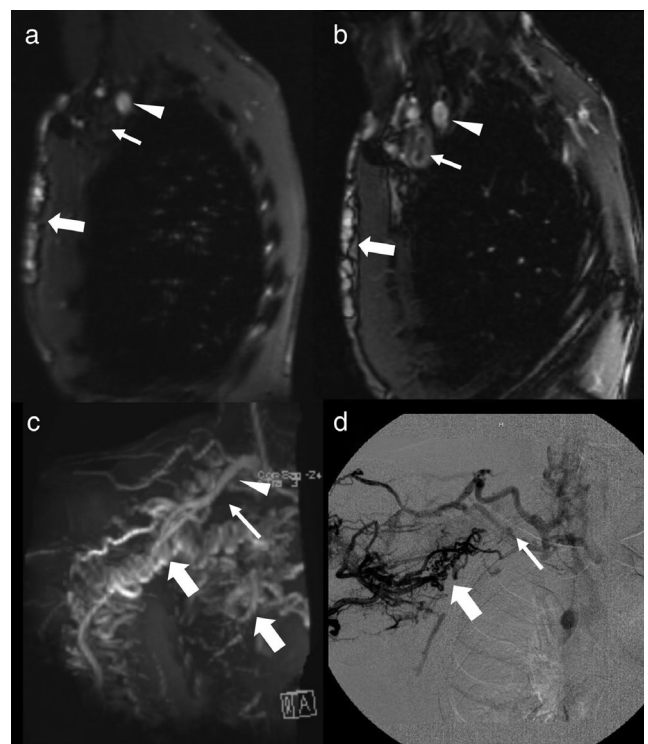
FIGURE 13: TOF MRA of right subclavian vein occlusion in a 40-year-old man with end-stage renal disease and a right arm arteriovenous fistula. Sagittal TOF MR angiographic image (a) demonstrates a lack of flow in the right subclavian vein (thin arrow), just inferior to the right subclavian artery, which is patent (arrowhead). Multiple enlarged venous collateral vessels are noted along the right anterior chest (thick arrows). Corresponding sagittal bSSFP MR image (b) shows heterogeneous signal within an expanded right subclavian vein (thin arrow), consistent with thrombosis. Coronal MIP TOF MRA image (c) again shows a lack of flow in the expected location of the right subclavian vein (thin arrow) and multiple venous collateral vessels (thick arrows). These findings were confirmed with catheter venography (d).
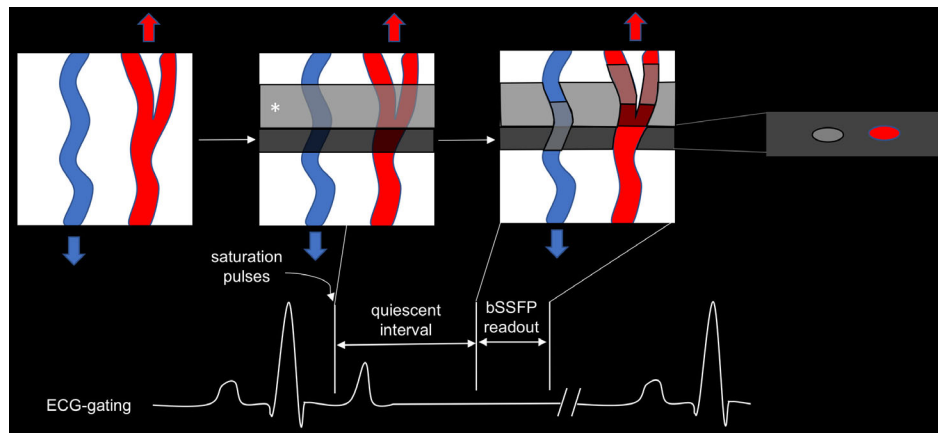
FIGURE 14: Mechanism of contrast in QISS MRA. Using ECG-triggering, a slice-selective RF saturation pulse is used to null the tissues in the imaging section shortly after the R-wave (ie, 100 msec delay). Additionally, a second saturation pulse is used above or below the imaging section to suppress venous inflow (asterisk). A quiescent interval occurs, allowing of the inflow of unsaturated arterial blood during systole. Imaging occurs during diastole of the same heartbeat, in which arterial flow is minimal or slow. A single-shot bSSFP technique is used for readout owing to its rapid acquisition speed. The result is a nonsubtractive MRA image acquired in a single heartbeat.

imaging and the ability to image during breath-holding, QISS MRA is inherently less sensitive to cardiac motion, pulsation artifacts, and respiratory motion. Similar to TOF MRA, QISS can be used for venous imaging, by flipping the orientation of the inflow suppression pulse and increasing the quiescent interval to provide more time for venous inflow.[53] Other less commonly used forms of inflow-enhanced bSSFP sequences exist (ie, noncontrast MRA of arteries and veins using sampling perfection with application optimized contrasts using different flip angle evolution and true fast imaging with steady-state precession [NATIVE TrueFISP], inhance inflow IR [IFIR], balanced triggered angiography non-contrast enhanced [B-TRANCE]), which are conceptually similar to QISS and leverage arterial inflow and a bSSFP readout to achieve a high signal within arterial blood.[56]

As with TOF, QISS has poor sensitivity for in-plane flow, as it requires inflow of unsaturated blood. Thus, QISS is optimized for peripheral imaging, in which the arteries are perpendicular to the plane of imaging.[57] However, due to its increased sensitivity for slow through-plane flow, QISS MRA is well suited for noncontrast imaging of the thoracic vasculature (Fig. 15). An important limitation to QISS is the appearance of off-resonance artifacts attributable to the bSSFP readout, which can be minimized by imaging at the magnet isocenter and performing automatic reshimming when multiple stations are used.[53,54]

Subtractive 3D MRA

In spin-echo imaging, flow-related signal loss occurs in vessels with brisk flow owing to motion out of the imaging slice between the 90° excitation pulse and the 180° refocusing pulse (ie, spin dephasing). This effect is most pronounced in the setting of rapid flow, and arterial flow during systole causes the highest degree of spin dephasing. ECG-gated subtractive 3D fast spin-echo (FSE), also known as fresh blood imaging (ie, noncontrast MRA of arteries and veins using sampling perfection with application optimized contrasts using different flip angle evolution [NATIVE SPACE], inhance deltaflow, triggered angiography noncontrast enhanced [TRANCE]), is an MRA technique that utilizes differences in spin dephasing between systole and diastole to create bright-blood images.[58–60] Using ECG-gating, a fast spin-echo (FSE) readout is performed during systole and diastole for a 3D slab, and the systolic images, in which flowing
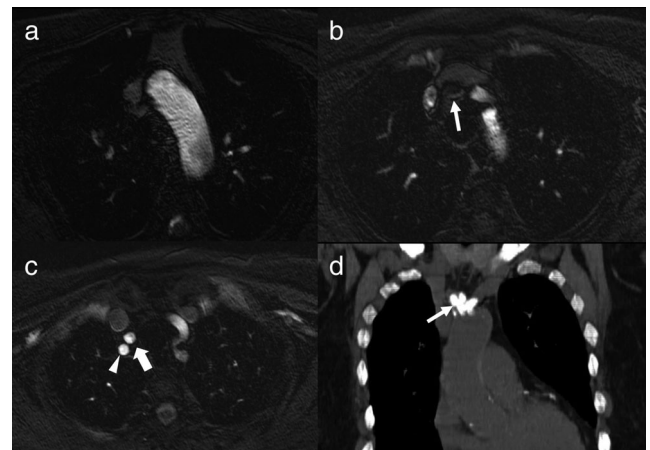
FIGURE 15: QISS MRA of high-grade innominate artery stenosis or occlusion in a 77-year-old woman with severe chronic kidney disease who was admitted with a right cerebral hemispheric infarction. Sequential QISS MRA images (a–c) demonstrate minimal to no flow in the innominate artery (thin arrow), with reconstitution of the right subclavian artery (arrowhead) and right common carotid artery (thick arrow) distally. Coronal non-contrast MIP CT image (d) demonstrates extensive calcification involving the origin of the innominate artery (thin arrow). The patient was managed with a surgical aorto-innominate arterial bypass procedure.
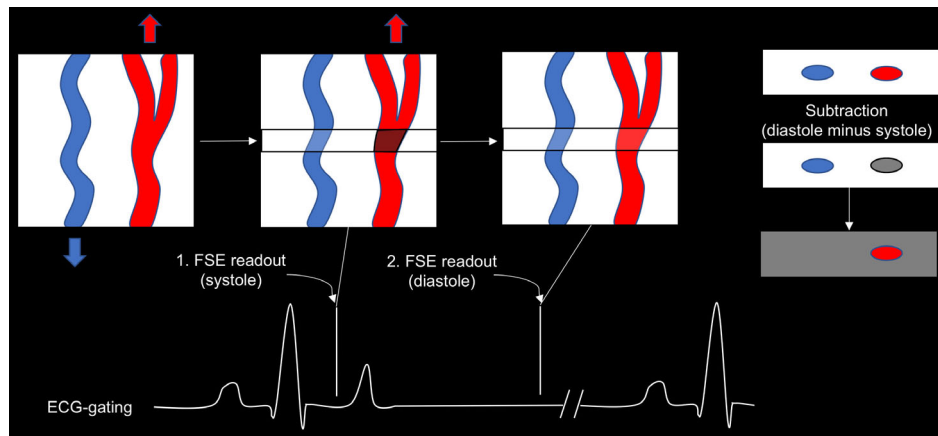
FIGURE 16: Mechanism of contrast in ECG-gated subtractive FSE MRA. Preparatory pulses are first performed to ascertain the optimal delay between the R-wave and peak systolic and minimal diastolic flow. Subsequently, ECG gating is used to acquire a 3D slab during systole and diastole. Spin dephasing results in luminal flow voids that are most pronounced in the arteries during systole. The systolic 3D acquisition, in which patient arteries are dark, is subtracted from the diastolic acquisition, in which arteries and veins are bright, to create a 3D MRA image with venous and background suppression.

arteries harbor luminal flow voids, are subtracted from the diastolic images to create a 3D MRA image with venous suppression and a high degree of background suppression (Fig. 16). Preparatory scans are required before data acquisition to determine the appropriate trigger delays for optimal systolic and diastolic imaging.[13]

In contradistinction to QISS, ECG-gated subtractive FSE avoids the off-resonant artifacts encountered during the bSSFP readout.[53] Additionally, ECG-gated subtractive FSE has a high sensitivity for slow flow, and thus is used most commonly for peripheral MRA. However, ECG-gated subtractive FSE also has potential applications for thoracic aortic imaging. When imaging a large vessel such as the aorta, venous and background suppression are less of a concern, and generally only the diastolic acquisition is required.[13] Important limitations of ECG-gated subtractive FSE include sensitivity to arrhythmias, requirement for preparatory sequences, and misregistration artifacts related to patient motion between the systolic and diastolic acquisition.[13,61] Physician monitoring is generally required to determine optimal timing delays for the systolic and diastolic phases, which can be further complicated by the presence of upstream stenosis when imaging distal vessels, although this is generally less of a concern in thoracic imaging. Additionally, acquisition times are typically longer than bSSFP-based techniques, and require 2–3 minutes for each 3D acquisition.

Arterial spin labeling (ASL) is another subtractive 3D MRA technique, in which one acquisition is performed after a saturation band is applied upstream of the arterial inflow, resulting in intraluminal signal loss within the patient arteries. A second acquisition is performed on the same slice without the use of the preparatory saturation band, and subtraction is performed to create bright-blood MRA images, in a similar fashion to ECG-gated subtractive FSE (Fig. 17).[36] ASL can

be used with a bSSFP readout, or in combination with an ECG-gated subtractive FSE technique.[62,63] ASL-based techniques are most commonly employed for brain perfusion imaging[53]; however, ASL has also been applied to visceral arterial, portal venous, and hepatic venous angiography.[64–67] While not often currently utilized for thoracic imaging, a potential application of ASL would be MRA of the great vessels of the chest and neck. ASL offers a high degree of background and venous suppression. Important limitations include increased acquisition times, reliance on subtraction for background suppression, and possible overestimation of stenosis related to decreased arterial signal in the setting of slow arterial inflow.[36]
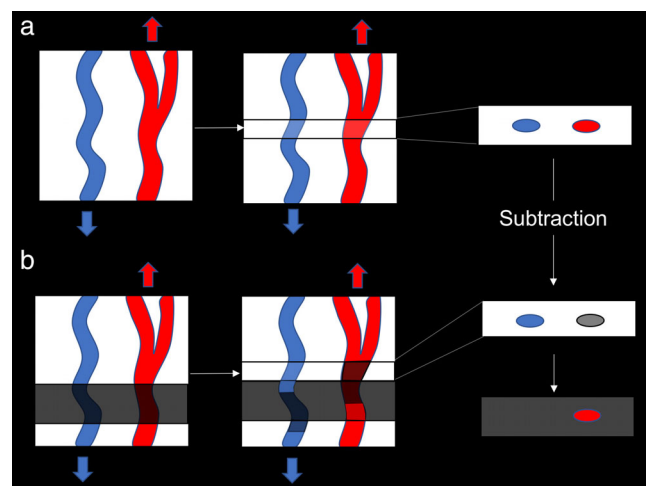

FIGURE 17: Mechanism of contrast in ASL. Two sequential acquisitions are performed, without and with a saturation band applied upstream of the arterial inflow (a,b, respectively). With the saturation band applied, intraluminal signal is suppressed within the patent artery. Subtraction is used to create a bright-blood MRA image.

Phase-Contrast Imaging

Phase contrast (PC) imaging is a powerful functional technique used for imaging blood flow and is most commonly used in the assessment of flow velocity and direction. In PC imaging, bipolar gradients (ie, a pair of gradients with opposite polarity) of equal strength are applied in succession.[68,69] Stationary protons are dephased and completely rephased, and thus experience no net phase shift. However, moving protons experience a net phase shift, which is directly proportional to the speed that a proton is moving in the direction the bipolar gradients are applied. Magnetic field inhomogeneity has the potential to introduce phase shifts that are not attributable to proton motion, and thus separate acquisitions are performed using two different bipolar gradients, one of which is a flow-encoding gradient (ie, velocity-encoding gradient [VENC]) and another which is a flow-compensated gradient.[15] Three flow-encoding acquisitions, one in each of three orthogonal directions, and one flow-compensated acquisition in all three directions are used to produce a pair of datasets that are subtracted from one another, serving to reduce artifactual phase shifts. PC imaging produces a phase image, in which the signal intensity of the image can be used to calculate flow velocity in the direction of the flow-encoding gradient.[70] Magnitude images are also reconstructed to provide an anatomic reference image (Fig. 18). The operator must choose a VENC prior to the acquisition, which corresponds to a phase shift of 180°, and represents the maximum and minimum measurable flow velocity. When flow velocity exceeds the VENC, aliasing occurs (Fig. 19). If the VENC is set substantially higher than maximum flow velocity, sensitivity for slow flow is decreased.[15] Thus, the ideal VENC is slightly higher than the expected maximum flow velocity.

PC imaging is most commonly used in the thorax for assessing flow velocities in the aorta and pulmonary artery, as well as for quantifying the severity of valvular disease (Fig. 19). PC may also be useful for the assessment of functional biomarkers of vessel stiffness such as pulse wave velocity, which may aid in the prognostication of cardiovascular disease.[71] Key strengths of PC imaging are a high degree of background suppression and the ability to calculate flow velocity. An important consideration in PC imaging is the selection of the imaging plane, which must be prescribed at the time of the imaging acquisition. Flow quantification is most accurate when the imaging plane is perpendicular to the vessel of interest and through-plane flow is used for encoding; however, peak velocity is best assessed using a plane perpendicular to a stenotic flow jet, when present.[72] Important limitations of PC imaging include sensitivity to motion due to subtraction of the flow-compensated dataset, as well as overestimation of the degree of stenosis due to intravoxel dephasing.[13]

4D Flow Imaging

When PC imaging is performed with a volumetric acquisition and 3D velocity encoding, PC MRA images can be produced, in which the signal intensity is proportional to blood velocity, regardless of the flow direction.[73] In conjunction with ECG gating (ie, 3D cine or 4D flow), complex flow dynamics can be depicted.[74] 4D flow data are typically visualized using 3D
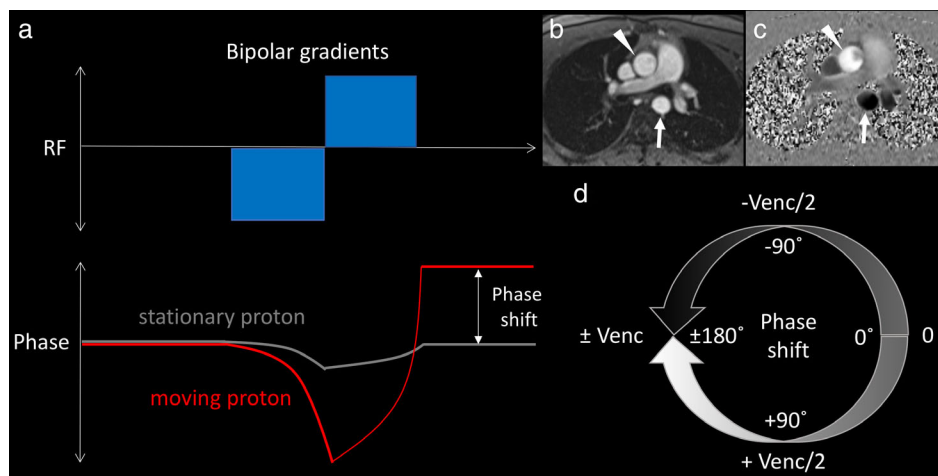
FIGURE 18: Mechanism of contrast in PC imaging. Bipolar gradients of equal strength are applied in succession, which serve to dephase and subsequently rephase the spins of stationary protons (a, gray curve). However, a proton experiences a net phase shift proportional to its velocity (a, red curve). PC imaging generates a magnitude image (b), in which the intensity is proportional to the net velocity of flow within each voxel, regardless of the flow direction, and a phase image (c), in which the signal intensity is proportional to the accumulated phase shift (c). Note that on the magnitude image, both the ascending thoracic aorta (arrowhead) and the descending thoracic aorta (arrow) have a high signal intensity. However, on the phase image the ascending aorta has bright signal intensity indicative of fast caudal-to-cranial flow, whereas the descending aorta has a low signal intensity indicative of fast cranial-to-caudal flow. Flow velocity and direction can be calculated from the signal intensity on the phase images by accounting for the strength of the VENC and degree of phase shift (d). When the VENC is set too low, aliasing can occur owing to the continuous nature of the phase shift.
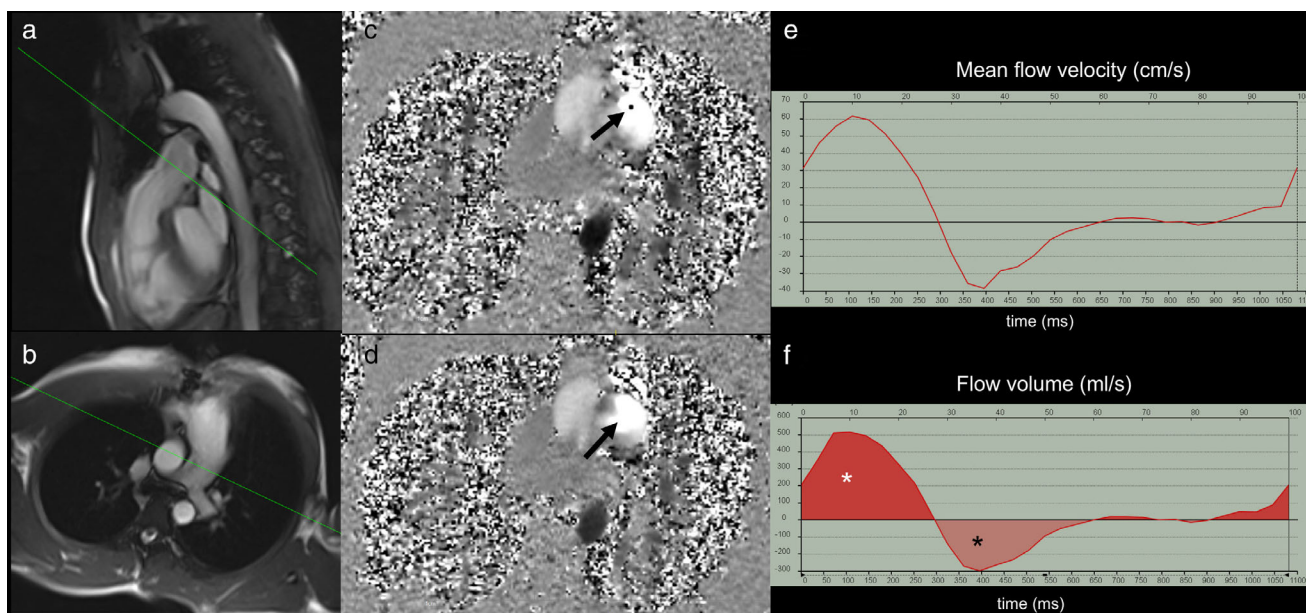
FIGURE 19: PC imaging of pulmonic regurgitation in a 16-year-old boy with tetralogy of Fallot who underwent surgical repair at 4 months of age. PC imaging of the pulmonary artery was performed by setting up a perpendicular scan plane on bSSFP oblique sagittal (a) and oblique axial (b) MR images. Phase images obtained using a VENC gradient of 150 cm/s (c) show a focal transition from high signal intensity to low signal intensity (arrow), consistent with aliasing. This was corrected using a VENC of 200 cm/s (d), and peak velocity was 180 cm/s. Phase contrast images can be used to generate quantitative flow parameters including mean flow velocity (e) and flow volume (f). The area under the positive portion of the flow volume curve (white asterisk) denotes forward flow volume, whereas the areas under the negative portion of the curve (black asterisk) denotes reverse flow volume. The regurgitant fraction was calculated at nearly 50%. The patient was managed with a transcatheter pulmonic valve replacement.

streamlines or time-resolved 3D particle traces. 4D flow imaging may aid in the evaluation of aortic dissection by depicting flow within the false lumen and portraying hemodynamically active fenestrations (Fig. 20).[75] Additional applications include visualizing flow dynamics within an aortic aneurysm, assessment of the hemodynamic significance of an aortic coarctation, and evaluation of valve-related disease of the ascending aorta.[73,76–78] Furthermore, flow velocity can be retrospectively calculated for any vessel or cardiac valve in any plane of choice after the entire 3D volume is acquired, obviating an important limitation of traditional 2D PC imaging.[79,80]

Currently, 4D flow imaging is infrequently used due to the long acquisition times that are required, typically on the order of 10–15 minutes. However, incorporation of compressed sensing techniques may substantially shorten the duration of acquisition and facilitate its integration into clinical practice.[81] Furthermore, the use multiple VENC parameters may improve the precision of the 4D flow technique, by increasing the range of velocities that can be reliability measured in a single acquisition.[82–84]

Dark-Blood Imaging

Dark-blood (or black-blood) images, while not used for angiography, are used routinely in the setting of a thoracic MRA examination. As described above, flow-related signal loss occurs in flowing vessels on spin-echo images due to spin dephasing. Double inversion recovery is a commonly used ECG-gated technique that results in improved suppression of the intraluminal signal.[85,86] Two consecutive 180° inversion pulses are applied; the first is a nonselective pulse applied to the entire imaging volume, whereas the second is a slice-selective pulse applied in early systole. A readout is performed in diastole, typically using a single-shot FSE technique, which allows for sufficient inflow of suppressed blood and is timed to coincide with the approximate inversion time of blood (ie, 650 msec) (Fig. 21).[15] Anatomic coverage of the entire thorax can typically be obtained in 1–3 breath-holds, depending on the slice thickness required.

Dark-blood imaging is most useful in detecting mural vascular abnormalities such as intramural hematoma, in which the hematoma may be difficult to distinguish from the aortic lumen on contrast-enhanced MRA images (Fig. 22).[13] Additionally, dark-blood imaging can aid in the detection of intraluminal abnormalities such as a dissection flap, vascular thrombosis, and even pulmonary embolism (Fig. 23). Dark-blood images are often useful for identifying abnormalities in the mediastinum, lung, and surrounding soft tissues.[24] The use of a 3D technique and addition of respiratory navigation has the potential to provide images of high spatial resolution (ie, <1 mm), and has recently been used to identify coronary aneurysms in patients with Kawasaki disease.[87] An important limitation of dark-blood imaging is the potential for slow flow to mimic thrombosis, owing to insufficient inflow of suppressed blood.[36] However, this phenomenon can also be
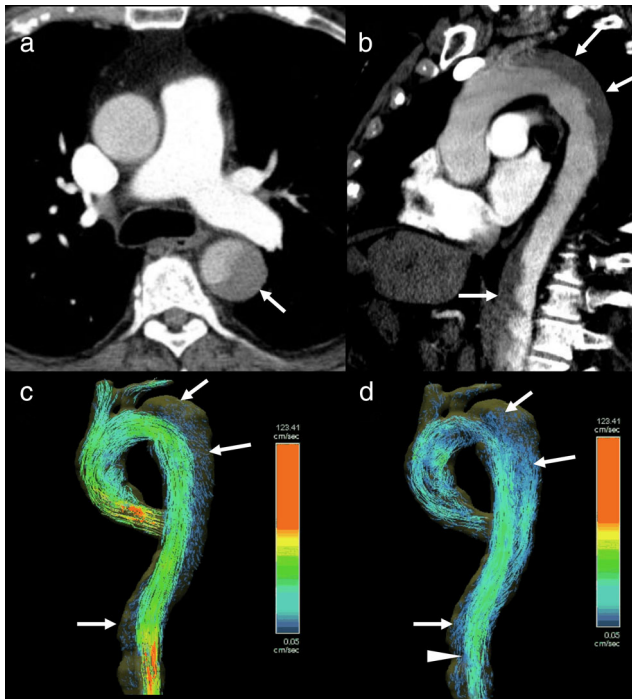
FIGURE 20: 4D flow imaging of Type B aortic dissection with a patent false lumen in a 71-year-old man presenting with chest pain. Transaxial and oblique sagittal contrast-enhanced CT images (a,b, respectively) show a Type B dissection with arch involvement extending distally to the level of the renal arteries (arrows). Due to the relative hypoenhancement on CT imaging, the false lumen was thought to be thrombosed. 3D ECG-gated PC (ie, 4D flow) oblique sagittal volume-rendered images in systole and early diastole (c,d, respectively) show retrograde flow within the false lumen, which is apparent during diastole (arrows, d) but not systole (arrows c). Additionally, backfilling of the false lumen occurs via a single distal entry tear (arrowhead). These findings confirm false lumen patency and demonstrate flow dynamics within the dissection. Conservative management was pursued.

used as a potential diagnostic tool. For instance, the severity of slow-flow artifact on dark-blood imaging of the pulmonary arteries has been used to estimate the severity of pulmonary hypertension.[88]

PROTOCOL DEVELOPMENT

Thoracic MRA is a robust approach to evaluate the thoracic vasculature in properly selected patients. Table 2 shows representative protocols used at our institution for a variety of thoracic applications, with the most important sequences in each protocol shown in bold. An important decision point is whether contrast can be administered. Contrast should be given to any patient without a specific contraindication, as it allows for rapid multiphasic imaging with a high SNR, and increases the diagnostic confidence of the evaluation. As described above, important contraindications to GBCA include advanced chronic kidney disease and acute renal failure; additional contraindications include pregnancy and a prior immediate adverse reaction to a GBCA of at least moderate severity.[6] In patients who cannot receive GBCAs, noncontrast MRA techniques are often sufficient to address many clinical questions, such as whether the patient harbors acute aortic pathology.

When contrast is administered, the next question is what phases of contrast are needed. Most frequently, a first-pass arterial phase is performed after a test bolus injection, and several delayed phases of contrast are obtained to confirm significant findings and provide additional opportunities to evaluate the arterial anatomy, should the patient move during the first acquisition or the bolus be missed. Delayed-phase images (ie, 5 minutes after injection) are often useful to evaluate for inflammatory conditions such as vasculitis or perivasculitis (Fig. 4). Provocative maneuvers
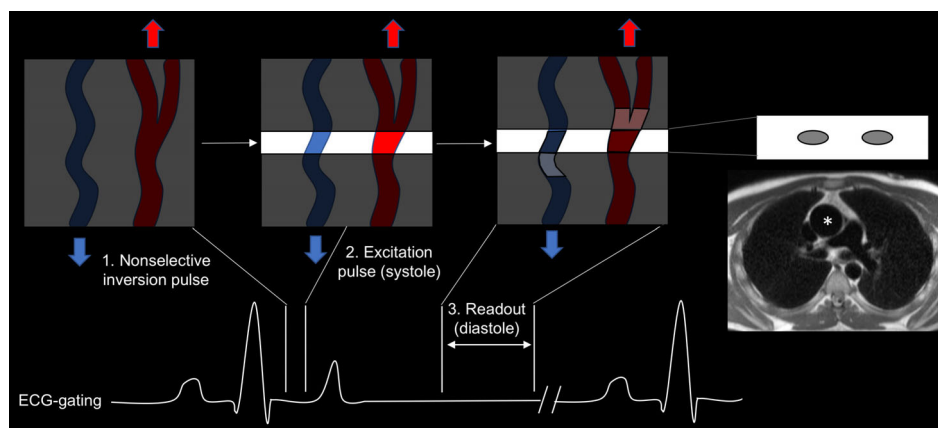
FIGURE 21: Mechanism of noncontrast double inversion recovery dark-blood imaging. A nonselective inversion pulse is first applied to the entire imaging volume. Next, a second slice-selective pulse is applied in early systole using ECG-gating, in order to restore longitudinal magnetization within the imaging slice. Finally, a readout is performed in diastole, typically using a single-shot FSE technique, which is timed to coincide with the inversion time of blood (ie, ~650 msec), and additionally allows for sufficient inflow of suppressed blood. The resultant image results in complete suppression of the intraluminal signal (asterisk).

FIGURE 22: Black-blood MRI of Type B aortic intramural hematoma in a 65-year-old woman presenting with chest pain. Transaxial and oblique sagittal black-blood single-shot FSE MR images (a,b, respectively) demonstrates a smooth crescent of high signal intensity within the wall of the descending thoracic aorta (arrows), extending from just distal to the takeoff of the left subclavian artery inferiorly to at least the diaphragmatic hiatus, consistent with a Type B intramural hematoma. A high-attenuation crescent is seen at this location on a contemporaneous transaxial noncontrast CT image (c, arrow). Notably, the intramural hematoma is more difficult to appreciate on the contrast-enhanced oblique sagittal MRA image (d, arrows). The patient was managed with aggressive blood pressure control, and her intramural hematoma progressively decreased in size and eventually resolved over the next 4 years.

FIGURE 23: Black-blood MRI of incidental saddle pulmonary embolism in a 65-year-old man admitted with shortness of breath and congestive heart failure. Transaxial bla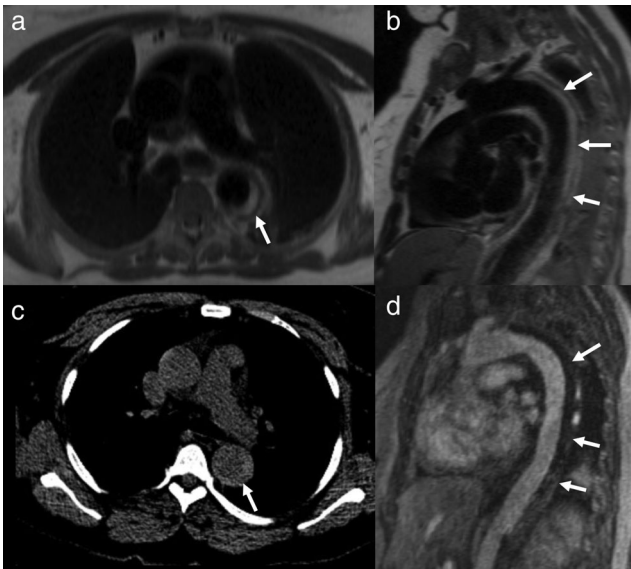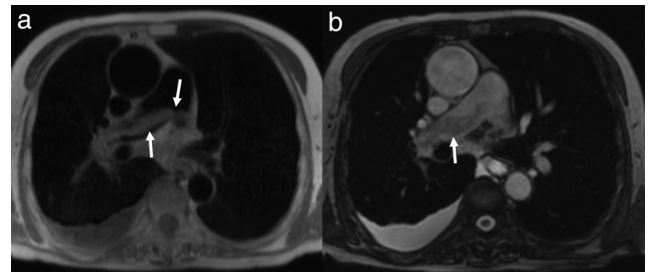ck-blood single shot FSE MR image (a) demonstrates a linear hyperintensity straddling the left and right pulmonary artery (arrows), consistent with saddle pulmonary embolism. Flowing blood in the pulmonary artery is hypointense on black-blood MR images, owing to the double-inversion technique. The pulmonary embolism is more difficult to appreciate on corresponding transaxial bSSFP single shot MR image (b, arrow) due to the more similar T_2/T_1 ratio between the thrombus and surrounding blood pool.

such as imaging with the arms abducted and adducted can be useful for assessment of position-dependent pathology, such as thoracic outlet syndrome (Fig. 24).[89,90] Another important question is whether ECG and/or respiratory gating is required. ECG gating is used in multiple noncontrast MRA techniques, and can be added to contrast-enhanced MRA sequences when needed, such as for evaluation of the aortic root. In patients unable to hold their breath, respiratory gating or a radial k-space acquisition can be employed in many contrast-enhanced and noncontrast MRA techniques. Additionally, when functional imaging such as flow parameters are required, specifically for evaluating the pressure gradient across an aortic coarcation or cardiac valve, 2D PC imaging is typically performed.[91] Finally, the application of 4D flow techniques, while not widely used in clinical practice due to long acquisition times, may prove useful for depiction of aortic flow dynamics and comprehensive assessment of cardiac valves.

Evaluation of the Acute Aorta

Evaluation for acute aortic pathology is the most common indication for urgent thoracic MRA at our institution.

Coronal T_2-weighted single-shot (SS)-FSE imaging is performed at the outset of the exam to assist in the determination of imaging coverage and localize anatomy of interest. Next, black-blood images using a SS-FSE technique are obtained in the axial, coronal, and oblique sagittal planes to identify mural vascular pathology such as intramural hematoma or mural wall thickening. Subsequently, transverse single-shot bSSFP images are obtained for anatomic assessment of the heart and great vessels. If contrast is not administered, transverse bSSFP cine images are acquired at single levels throughout the entire thoracic aorta, to aid in the depiction of an aortic dissection flap. Coronal bSSFP cine images are acquired to profile the aortic root and evaluate the aortic valve. Inversion recovery imaging is included at two selected levels to depict intramural and perivascular edema. Additionally, whether or not contrast is administered, volume-interpolated GRE imaging is performed in the transverse plane to aid in the assessment for intramural hematoma and to evaluate for blood products outside the vasculature.

Contrast is administered whenever possible, as it shortens the overall duration of the exam by eliminating the need for transverse bSSFP cine imaging of the entire thoracic aorta. MRA images are acquired in the oblique sagittal plane prior to (ie, mask) and following contrast administration in the arterial and two immediately delayed phases, ensuring at least one acquisition will provide adequate arterial opacification and be relatively free of motion. All three postcontrast MRA image sets are postprocessed by mask subtraction and creation of a thick-slice MIP image. Most commonly, the unmasked MRA images are used for diagnosis, whereas the mask subtracted images are used for MIP generation, which highlight any vascular findings and are useful for summarizing findings to the referring clinician. Subsequently, postcontrast transverse volume-interpolated GRE images are

TABLE 2. Example Thoracic Vascular MRA Imaging Protocols

Indications	Technique	Basic sequences
Acute aortic pathology (noncontrast)	Coverage: Aortic arch through upper abdomen (optional coverage through femoral vessels) EKG gating: On Contrast: None	1. Localizer 2. Coronal T$_2$W SS-FSE 3. Transverse, coronal, and oblique sagittal black-blood SS-FSE 4. Transverse single-shot bSSFP stack 5. **Transverse bSSFP cine – at single levels through the entire thoracic aorta** 6. **Coronal bSSFP cine (aortic outflow tract)** 7. Transverse inversion recovery (two levels through ascending aorta) 8. Transverse 3D volume-interpolated GRE stack
Acute aortic pathology (with contrast)	Coverage: Aortic arch through upper abdomen (optional coverage through femoral vessels) EKG gating: On Contrast: Single dose at 2 cc/sec	1. Localizer 2. Coronal T$_2$W SS-FSE 3. Transverse and oblique sagittal black-blood SS-FSE 4. Transverse single-shot bSSFP stack 5. **Transverse bSSFP cine slices (aortic root and mid ascending)** 6. **Coronal bSSFP cine (aortic outflow tract)** 7. Transverse inversion recovery (two levels through ascending aorta) 8. Transverse 3D volume-interpolated GRE stack precontrast 9. Oblique sagittal 3D MRA mask 10. **Oblique sagittal 3D MRA postcontrast x3** 11. Transverse 3D volume-interpolated GRE stack postcontrast 12. Oblique sagittal subtractions with MIP images
Aortic measurements (noncontrast)	Coverage: Aortic arch through upper abdomen EKG gating: On Contrast: None	1. Localizer 2. Coronal T$_2$W SS-FSE 3. Transverse, coronal, and oblique sagittal black-blood SS-FSE 4. Transverse single-shot bSSFP stack 5. Transverse 3D volume-interpolated GRE stack 6. **Oblique sagittal 3D isotropic noncontrast MRA with ECG gating and respiratory navigation**
Aortic measurements (with contrast)	Coverage: Aortic arch through upper abdomen EKG gating: On Contrast: Single dose at 2 cc/sec	1. Localizer 2. Coronal T$_2$W SS-FSE 3. Transverse and oblique sagittal black-blood SS-FSE 4. Transverse single-shot bSSFP stack 5. Transverse 3D volume-interpolated GRE stack pre-contrast 6. Oblique sagittal 3D MRA mask 7. Oblique sagittal 3D MRA postcontrast x3 8. Transverse 3D volume-interpolated GRE stack postcontrast 9. **Oblique sagittal 3D isotropic MRA with ECG gating and respiratory navigation**
Aortitis (with contrast)	Coverage: Aortic arch through upper abdomen (optional coverage through aortic bifurcation) EKG gating: On	1. Localizer 2. Transverse and oblique sagittal black-blood SS-FSE 3. **Transverse inversion recovery stack** 4. Transverse single-shot bSSFP

TABLE 2. Continued

Indications	Technique	Basic sequences
	Contrast: Single dose at 2 cc/sec	5. Oblique sagittal 3D MRA Mask 6. Transverse 3D volume-interpolated GRE stack precontrast 7. **Transverse 3D volume-interpolated GRE stack postcontrast x2** 8. Oblique sagittal 3D MRA postcontrast x2 9. **Transverse 3D volume-interpolated GRE stack postcontrast (5 minute delay)**
MRA/MRV (with contrast)	Coverage: Chest EKG gating: Off Contrast: Single dose at 2 cc/sec	1. Localizer 2. Coronal T_2W SS-FSE 3. Coronal T_1W high resolution (including axilla) 4. Transverse T_1W high resolution FSE (upper chest) 5. Transverse 3D volume-interpolated GRE precontrast 6. Oblique sagittal 3D MRA Mask (including axilla) 7. **Oblique sagittal 3D MRA postcontrast x3** 8. Transverse 3D volume-interpolated GRE stack postcontrast
Thoracic outlet syndrome (with contrast)	Coverage: Chest EKG gating: Off Contrast: Single dose at 2 cc/sec; Half dose used with arms down, half dose used with arms up	1. Localizer (arms adducted) 2. Coronal and transverse T_1W high resolution FSE 3. Transverse 3D volume-interpolated GRE precontrast 4. Sagittal single-shot bSSFP 5. Coronal 3D MRA Mask 6. **Coronal 3D MRA postcontrast in arterial, venous, and equilibrium phases (use first half contrast dose)** 7. Sagittal 3D MRA postcontrast 8. Transverse 3D volume-interpolated GRE stack postcontrast 9. Localizer (arms abducted) 10. Coronal 3D MRA Mask 11. **Coronal 3D MRA postcontrast in arterial, venous, and equilibrium phases (use second half of contrast dose)** 12. Sagittal 3D MRA postcontrast 13. Transverse 3D volume-interpolated GRE stack postcontrast
Pulmonary embolism (with contrast)	Coverage: Chest EKG gating: On Contrast: Single dose at 2 cc/sec	1. Localizer 2. Coronal 3D MRA Mask 3. Transverse 3D volume-interpolated GRE precontrast 4. **Coronal 3D MRA x3 (time first run for optimal pulmonary artery enhancement)** 5. Transverse 3D volume-interpolated GRE postcontrast 6. Transverse radial 3D spoiled GRE (non-breathhold)

obtained for further characterization of mural and extravascular pathology. Contrast-enhanced MRA images are not gated in this setting, and therefore may contain phase ghosting artifacts within the ascending aorta that can mimic a dissection flap. Transverse bSSFP cine imaging is performed at two selected levels in the ascending aorta to include the aortic root, primarily for interrogation of these potential phase ghosting artifacts. Coronal bSSFP cine images are similarly acquired for this purpose, and are additionally used for evaluation of the aortic valve.

If aortitis is known or strongly suspected, transverse volume-interpolated GRE stacks are acquired in the arterial,
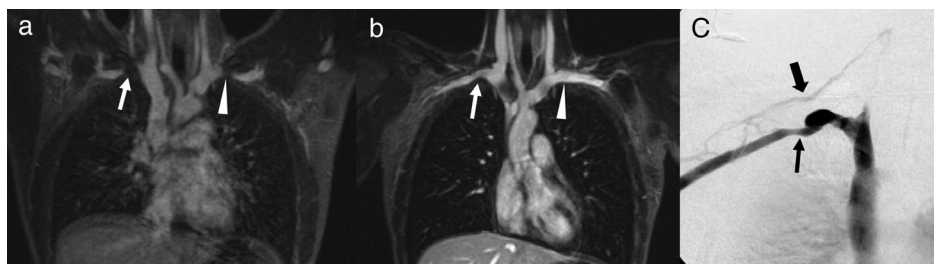
FIGURE 24: Utility of provocative maneuvers in contrast-enhanced MRA of venous thoracic outlet syndrome in a 16-year-old girl presenting with right arm swelling. Contrast-enhanced MRA images obtained with the arms abducted (a) demonstrate marked symmetric narrowing of both subclavian veins at the thoracic inlet (right: thin arrow; left: arrowhead). Contrast-enhanced MRA images obtained with the arms adducted (b) show mild fixed stenosis of the right subclavian vein (thin arrow), consistent with right-sided venous thoracic outlet syndrome. There is no fixed stenosis of the left subclavian vein (arrowhead). Intraoperative venographic image confirms the presence of right subclavian vein stenosis (thin arrow) and demonstrates filling of an enlarged collateral vein (thick arrow). The patient subsequently underwent right thoracic outlet decompression and patch angioplasty of the right subclavian vein.

venous, and 5-minute delayed phases, which better depict enhancement of the arterial wall and/or perivascular soft tissues compared with oblique sagittal MRA images. Additionally, an entire stack of transverse inversion recovery images, rather than just two levels, are obtained for more comprehensive evaluation. If aortic dissection is not suspected clinically, bSSFP cine imaging of the ascending aorta and aortic outflow tract is typically omitted.

Aortic Measurements

Evaluation of aortic size in the setting of known or suspected thoracic aortic aneurysm or prior dissection represents the most common indication for routine MRA at our institution. As in our acute aorta protocols, evaluation begins with coronal T_2-weighted SS-FSE images, and further includes axial, coronal, and oblique sagittal black-blood images, as well as transverse single-shot bSSFP images. These sequences aid in the depiction of aneurysm instability or intramural hematoma, and assist in the characterization of extravascular abnormalities. Transverse volume-interpolated GRE imaging is also performed to aid in the depiction of intramural hematoma. If contrast is not administered, noncontrast MRA is performed using a bSSFP technique using ECG and respiratory gating in the oblique sagittal plane, which typically requires 5–7 minutes. Isotropic voxels are prescribed, which allows for distortion-free MPRs of the aorta that are used to generate double-oblique measurements of the luminal aorta.

If contrast is administered, oblique sagittal MRA images are acquired before and after contrast administration in the arterial and two immediately delayed phases. Subtractions are performed and thick-slice MIP image generated, in a similar manner to our acute aorta protocol. Postcontrast transverse volume-interpolated GRE images are similarly obtained. In analogous fashion to our noncontrast aortic measurements protocol, ECG and respiratory gated contrast-enhanced MRA is performed in the oblique sagittal plane using an isotropic acquisition. Although this sequence requires a similar amount of time as the noncontrast ECG and respiratory gated MRA

acquisition, images after contrast often have substantially greater contrast-to-noise.

CONCLUSION

MRA is an established technique for evaluation of the thoracic vasculature. In general, contrast-enhanced MRA should be performed unless there is a specific contraindication to GBCAs, as it shortens the duration of the exam and increases the diagnostic confidence of the evaluation. Contrast timing for the first-pass arterial phase of contrast is frequently performed using a test bolus technique; however, time-resolved MRA has emerged as a robust alternative and has no requirement for precise contrast timing. A wide variety of non-contrast MRA techniques exist, each with its own set of strengths and disadvantages. Bright-blood noncontrast MRA techniques are optimized for intraluminal evaluation, whereas dark-blood techniques perform best for evaluation of mural and extraluminal structures. An assortment of additional techniques can be employed to address specific clinical questions, and include delayed contrast-enhanced imaging, provocative maneuvers, ECG and respiratory gating, and PC imaging.

CONFLICTS OF INTEREST

The authors have no relevant relationships to disclose.

References

1. American College of Radiology, Committee on Drugs and Contrast Media. ACR manual on contrast media v10.3 [Internet]. 2018 Accessed on May 8, 2019. Available from: https://www.acr.org/Clinical-Resources/Contrast-Manual

2. Brenner DJ, Elliston CD, Hall EJ, Berdon WE. Estimated risks of radiation-induced fatal cancer from pediatric CT. AJR Am J Roentgenol 2001;176(2):289-296.

3. Prince MR. Gadolinium-enhanced MR aortography. Radiology 1994; 191(1):155-164.

4. Prince MR, Narasimham DL, Jacoby WT, et al. Three-dimensional gadolinium-enhanced MR angiography of the thoracic aorta. AJR Am J Roentgenol 1996;166(6):1387-1397.

5. Leung DA, Debatin JF. Three-dimensional contrast-enhanced magnetic resonance angiography of the thoracic vasculature. Eur Radiol 1997;7 (7):981-989.

6. Fraum TJ, Ludwig DR, Bashir MR, Fowler KJ. Gadolinium-based contrast agents: A comprehensive risk assessment. J Magn Reson Imaging 2017;46(2):338-353.

7. Daram SR, Cortese CM, Bastani B. Nephrogenic fibrosing dermopathy/nephrogenic systemic fibrosis: Report of a new case with literature review. Am J Kidney Dis 2005;46(4):754-759.

8. Deray G, Rouviere O, Bacigalupo L, et al. Safety of meglumine gadoterate (Gd-DOTA)-enhanced MRI compared to unenhanced MRI in patients with chronic kidney disease (RESCUE study). Eur Radiol 2013;23(5):1250-1259.

9. Lauenstein T, Ramirez-Garrido F, Kim YH, et al. Nephrogenic systemic fibrosis risk after liver magnetic resonance imaging with gadoxetate disodium in patients with moderate to severe renal impairment: Results of a prospective, open-label, multicenter study. Invest Radiol 2015;50(6): 416-422.

10. Michaely HJ, Aschauer M, Deutschmann H, et al. Gadobutrol in renally impaired patients: Results of the GRIP study. Invest Radiol 2017;52(1): 55-60.

11. Xiao Y-D, Paudel R, Liu J, Ma C, Zhang Z-S, Zhou S-K. MRI contrast agents: Classification and application (Review). Int J Mol Med 2016;38 (5):1319-1326.

12. Rapp JH, Wolff SD, Quinn SF, et al. Aortoiliac occlusive disease in patients with known or suspected peripheral vascular disease: Safety and efficacy of gadofosveset-enhanced MR angiography-multicenter comparative phase III study. Radiology 2005;236(1):71-78.

13. Raptis C, Fowler KJ, Narra VR. Magnetic resonance angiography: Technique. *Problem solving in cardiovascular imaging* (Abbara S, Kalva SP, Eds.). London: Elsevier Health Sciences; 2012.

14. Guglielmo FF, Mitchell DG, Gupta S. Gadolinium contrast agent selection and optimal use for body MRI. Radiol Clin North Am 2014;52(4): 637-656.

15. Lee VS, Cardiovascular MRI. *Physical principles to practical protocols.* Philadelphia: Lippincott Williams & Wilkins; 2006.

16. Riederer SJ, Fain SB, Kruger DG, Busse RF. 3D contrast-enhanced MR angiography using fluoroscopic triggering and an elliptical centric view order. Int J Cardiovasc Imaging 1999;15(2):117-129.

17. Wilman AH, Riederer SJ, King BF, Debbins JP, Rossman PJ, Ehman RL. Fluoroscopically triggered contrast-enhanced three-dimensional MR angiography with elliptical centric view order: Application to the renal arteries. Radiology 1997;205(1):137-146.

18. Maki JH, Prince MR, Londy FJ, Chenevert TL. The effects of time varying intravascular signal intensity and k-space acquisition order on three-dimensional MR angiography image quality. J Magn Reson Imaging 1996;6(4):642-651.

19. Earls JP, Shaves SC. MR angiography of the thoracic, abdominal, and extremity venous system. Magn Reson Imaging Clin N Am 1998;6(2): 417-435.

20. Earls JP, Rofsky NM, DeCorato DR, Krinsky GA, Weinreb JC. Breath-hold single-dose gadolinium-enhanced three-dimensional MR aortography: Usefulness of a timing examination and MR power injector. Radiology 1996;201(3):705-710.

21. Hargreaves B. Rapid gradient-echo imaging. J Magn Reson Imaging 2012;36(6):1300-1313.

22. Groves EM, Bireley W, Dill K, Carroll TJ, Carr JC. Quantitative analysis of ECG-gated high-resolution contrast-enhanced MR angiography of the thoracic aorta. AJR Am J Roentgenol 2007;188(2): 522-528.

23. Arpasi PJ, Bis KG, Shetty AN, White RD, Simonetti OP. MR angiography of the thoracic aorta with an electrocardiographically triggered breath-hold contrast-enhanced sequence. Radiographics 2000;20(1): 107-120.

24. Raptis CA, Ludwig DR, Hammer MM, et al. Building blocks for thoracic MRI: Challenges, sequences, and protocol design. J Magn Reson Imaging 2019;50(3):682-701.

25. Rofsky NM, Lee VS, Laub G, et al. Abdominal MRI with a volumetric interpolated breath-hold examination. Radiology 1999;212(3):876-884.

26. Chandarana H, Block TK, Rosenkrantz AB, et al. Free-breathing radial 3D fat-suppressed T_1-weighted gradient echo sequence: A viable alternative for contrast-enhanced liver imaging in patients unable to suspend respiration. Invest Radiol 2011;46(10):648-653.

27. Bustin A, Ginami G, Cruz G, et al. Five-minute whole-heart coronary MRA with sub-millimeter isotropic resolution, 100% respiratory scan efficiency, and 3D-PROST reconstruction. Magn Reson Med 2019;81 (1):102-115.

28. Shen D, Edelman RR, Robinson JD, et al. Single-shot coronary quiescent-interval slice-selective magnetic resonance angiography using compressed sensing: A feasibility study in patients with congenital heart disease. J Comput Assist Tomogr 2018;42(5):739-746.

29. Nakamura M, Kido T, Kido T, et al. Non-contrast compressed sensing whole-heart coronary magnetic resonance angiography at 3T: A comparison with conventional imaging. Eur J Radiol 2018;104:43-48.

30. Riederer SJ, Haider CR, Borisch EA, Weavers PT, Young PM. Recent advances in 3D time-resolved contrast-enhanced MR angiography. J Magn Reson Imaging 2015;42(1):3-22.

31. Willinek WA, Hadizadeh DR, von Falkenhausen M, et al. 4D time-resolved MR angiography with keyhole (4D-TRAK): More than 60 times accelerated MRA using a combination of CENTRA, keyhole, and SENSE at 3.0T. J Magn Reson Imaging 2008;27(6):1455-1460.

32. Kramer U, Ernemann U, Fenchel M, et al. Pretreatment evaluation of peripheral vascular malformations using low-dose contrast-enhanced time-resolved 3D MR angiography: Initial results in 22 patients. AJR Am J Roentgenol 2011;196(3):702-711.

33. Benson DG, Schiebler ML, Repplinger MD, et al. Contrast-enhanced pulmonary MRA for the primary diagnosis of pulmonary embolism: Current state of the art and future directions. Br J Radiol 2017;90(1074): 20160901.

34. Blackham KA, Passalacqua MA, Sandhu GS, Gilkeson RC, Griswold MA, Gulani V. Applications of time-resolved MR angiography. AJR Am J Roentgenol 2011;196(5):W613-W620.

35. Quint LE, Liu PS, Booher AM, Watcharotone K, Myles JD. Proximal thoracic aortic diameter measurements at CT: Repeatability and reproducibility according to measurement method. Int J Cardiovasc Imaging 2013;29(2):479-488.

36. Morita S, Masukawa A, Suzuki K, Hirata M, Kojima S, Ueno E. Unenhanced MR angiography: Techniques and clinical applications in patients with chronic kidney disease. Radiographics 2011;31(2): E13-E33.

37. Fuchs F, Laub G, Othomo K. TrueFISP—Technical considerations and cardiovascular applications. Eur J Radiol 2003;46(1):28-32.

38. Scheffler K, Lehnhardt S. Principles and applications of balanced SSFP techniques. Eur Radiol 2003;13(11):2409-2418.

39. Haacke EM, Tkach JA. Fast MRI: Techniques and clinical applications. AJR Am J Roentgenol 1990;155(5):951-964.

40. Veldhoen S, Behzadi C, Lenz A, et al. Non-contrast MR angiography at 1.5 Tesla for aortic monitoring in Marfan patients after aortic root surgery. J Cardiovasc Magn Reson 2017;19(1):82.

41. François CJ, Tuite D, Deshpande V, Jerecic R, Weale P, Carr JC. Pulmonary vein imaging with unenhanced three-dimensional balanced steady-state free precession MR angiography: Initial clinical evaluation. Radiology 2009;250(3):932-939.

42. Krishnam MS, Tomasian A, Malik S, et al. Three-dimensional imaging of pulmonary veins by a novel steady-state free-precession magnetic resonance angiography technique without the use of intravenous contrast agent: Initial experience. Invest Radiol 2009; 44(8):447-453.

43. Krishnam MS, Tomasian A, Deshpande V, et al. Noncontrast 3D steady-state free-precession magnetic resonance angiography of the whole chest using nonselective radiofrequency excitation over a large field of view: Comparison with single-phase 3D contrast-enhanced magnetic resonance angiography. Invest Radiol 2008;43(6):411-420.

44. François CJ, Tuite D, Deshpande V, Jerecic R, Weale P, Carr JC. Unenhanced MR angiography of the thoracic aorta: initial clinical evaluation. AJR Am J Roentgenol 2008;190(4):902-906.

45. Götte MJW, Rüssel IK, de Roest GJ, et al. Magnetic resonance imaging, pacemakers and implantable cardioverter-defibrillators: Current situation and clinical perspective. Neth Heart J 2010;18(1):31-37.

46. Roguin A, Zviman MM, Meininger GR, et al. Modern pacemaker and implantable cardioverter/defibrillator systems can be magnetic resonance imaging safe. Circulation 2004;110(5):475-482.

47. Stadler A, Schima W, Ba-Ssalamah A, Kettenbach J, Eisenhuber E. Artifacts in body MRI: Their appearance and how to eliminate them. Eur Radiol 2007;17(5):1242-1255.

48. Saloner D. The AAPM/RSNA physics tutorial for residents. An introduction to MR angiography. Radiographics 1995;15(2):453-465.

49. Willinek WA, Born M, Simon B, et al. Time-of-flight MR angiography: Comparison of 3.0-T imaging and 1.5-T imaging—Initial experience. Radiology 2003;229(3):913-920.

50. Carr JC, Carroll TJ. Magnetic resonance angiography: Principles and applications. New York: Springer Science & Business Media; 2011.

51. Grayev A, Shimakawa A, Cousins J, Turski P, Brittain J, Reeder S. Improved time-of-flight magnetic resonance angiography with IDEAL water-fat separation. J Magn Reson Imaging 2009;29(6):1367-1374.

52. Ko S-F, Wan Y-L, Ng S-H, et al. MRI of thoracic vascular lesions with emphasis on two-dimensional time-of-flight MR angiography. Br J Radiol 1999;72(858):613-620.

53. Edelman RR, Koktzoglou I. Noncontrast MR angiography: An update. J Magn Reson Imaging 2019;49(2):355-373.

54. Edelman RR, Sheehan JJ, Dunkle E, Schindler N, Carr J, Koktzoglou I. Quiescent-interval single-shot unenhanced magnetic resonance angiography of peripheral vascular disease: Technical considerations and clinical feasibility. Magn Reson Med 2010;63(4):951-958.

55. Saini A, Wallace A, Albadawi H, et al. Quiescent-interval single-shot magnetic resonance angiography. Diagnostics (Basel) 2018;8(4): pii: E84.

56. Dong HZ, Worters PW, Wu HH, Ingle RR, Vasanawala SS, Nishimura DG. Non-contrast-enhanced renal angiography using multiple inversion recovery and alternating TR balanced steady state free precession. Magn Reson Med 2013;70(2):527-536.

57. Hodnett PA, Koktzoglou I, Davarpanah AH, et al. Evaluation of peripheral arterial disease with nonenhanced quiescent-interval single-shot MR angiography. Radiology 2011;260(1):282-293.

58. Meuli RA, Wedeen VJ, Geller SC, et al. MR gated subtraction angiography: Evaluation of lower extremities. Radiology 1986;159(2):411-418.

59. Miyazaki M, Sugiura S, Tateishi F, Wada H, Kassai Y, Abe H. Non-contrast-enhanced MR angiography using 3D ECG-synchronized half-Fourier fast spin echo. J Magn Reson Imaging 2000;12(5):776-783.

60. Miyazaki M, Takai H, Sugiura S, Wada H, Kuwahara R, Urata J. Peripheral MR angiography: Separation of arteries from veins with flow-spoiled gradient pulses in electrocardiography-triggered three-dimensional half-Fourier fast spin-echo imaging. Radiology 2003;227(3):890-896.

61. Lim RP, Hecht EM, Xu J, et al. 3D nongadolinium-enhanced ECG-gated MRA of the distal lower extremities: Preliminary clinical experience. J Magn Reson Imaging 2008;28(1):181-189.

62. Nishimura DG, Macovski A, Pauly JM, Conolly SM. MR angiography by selective inversion recovery. Magn Reson Med 1987;4(2):193-202.

63. Spuentrup E, Manning WJ, Börnert P, Kissinger KV, Botnar RM, Stuber M. Renal arteries: Navigator-gated balanced fast field-echo projection MR angiography with aortic spin labeling: Initial experience. Radiology 2002;225(2):589-596.

64. Wyttenbach R, Braghetti A, Wyss M, et al. Renal artery assessment with nonenhanced steady-state free precession versus contrast-enhanced MR angiography. Radiology 2007;245(1):186-195.

65. Shimada K, Isoda H, Okada T, et al. Non-contrast-enhanced hepatic MR angiography with true steady-state free-precession and time spatial labeling inversion pulse: Optimization of the technique and preliminary results. Eur J Radiol 2009;70(1):111-117.

66. Shimada K, Isoda H, Okada T, et al. Non-contrast-enhanced MR portography with time-spatial labeling inversion pulses: Comparison of imaging with three-dimensional half-Fourier fast spin-echo and true steady-state free-precession sequences. J Magn Reson Imaging 2009;29(5):1140-1146.

67. Shimada K, Isoda H, Okada T, et al. Non-contrast-enhanced MR angiography for selective visualization of the hepatic vein and inferior vena cava with true steady-state free-precession sequence and time-spatial labeling inversion pulses: Preliminary results. J Magn Reson Imaging 2009;29(2):474-479.

68. Bryant DJ, Payne JA, Firmin DN, Longmore DB. Measurement of flow with NMRI using a gradient pulse and phase difference technique. J Comput Assist Tomogr 1984;8(4):588-593.

69. Nayler GL, Firmin DN, Longmore DB. Blood flow imaging by cine magnetic resonance. J Comput Assist Tomogr 1986;10(5):715-722.

70. Markl M, Schnell S, Wu C, et al. Advanced flow MRI: Emerging techniques and applications. Clin Radiol 2016;71(8):779-795.

71. Wentland AL, Grist TM, Wieben O. Review of MRI-based measurements of pulse wave velocity: A biomarker of arterial stiffness. Cardiovasc Diagn Ther 2014;4(2):193-206.

72. Lotz J, Meier C, Leppert A, Galanski M. Cardiovascular flow measurement with phase-contrast MRI: Basic facts and implementation. Radiographics 2002;22(3):651-671.

73. Markl M, Frydrychowicz A, Kozerke S, Hope M, Wieben O. 4D flow MRI. J Magn Reson Imaging 2012;36(5):1015-1036.

74. Azarine A, Garçon P, Stansal A, et al. Four-dimensional flow MRI: Principles and cardiovascular applications. Radiographics 2019;39(3):632-648.

75. Allen BD, Aouad PJ, Burris NS, et al. Detection and hemodynamic evaluation of flap fenestrations in Type B aortic dissection with 4D flow MRI: Comparison with conventional MRI and CT angiography. Radiol Cardiothorac Imaging 2019;1(1):e180009.

76. Bogren HG, Mohiaddin RH, Yang GZ, Kilner PJ, Firmin DN. Magnetic resonance velocity vector mapping of blood flow in thoracic aortic aneurysms and grafts. J Thorac Cardiovasc Surg 1995;110(3):704-714.

77. Kozerke S, Hasenkam JM, Pedersen EM, Boesiger P. Visualization of flow patterns distal to aortic valve prostheses in humans using a fast approach for cine 3D velocity mapping. J Magn Reson Imaging 2001;13(5):690-698.

78. Garcia J, Barker AJ, Markl M. The role of imaging of flow patterns by 4D flow MRI in aortic stenosis. JACC Cardiovasc Imaging 2019;12(2):252-266.

79. Watanabe T, Isoda H, Fukuyama A, et al. Accuracy of the flow velocity and three-directional velocity profile measured with three-dimensional cine phase-contrast MRI: Verification on scanners from different manufacturers. Magn Reson Med Sci 2019;18(4):265-271.

80. van der Geest RJ, Garg P. Advanced analysis techniques for intra-cardiac flow evaluation from 4D flow MRI. Curr Radiol Rep 2016;4:38.

81. Ma LE, Markl M, Chow K, et al. Aortic 4D flow MRI in 2 minutes using compressed sensing, respiratory controlled adaptive k-space reordering, and inline reconstruction. Magn Reson Med 2019;81(6):3675-3690.

82. Sherrah AG, Callaghan FM, Puranik R, et al. Multi-velocity encoding four-dimensional flow magnetic resonance imaging in the assessment of chronic aortic dissection. Aorta (Stamford) 2017;5(3):80-90.

83. Callaghan FM, Kozor R, Sherrah AG, et al. Use of multi-velocity encoding 4D flow MRI to improve quantification of flow patterns in the aorta. J Magn Reson Imaging 2016;43(2):352-363.

84. Ha H, Kim GB, Kweon J, et al. Multi-VENC acquisition of four-dimensional phase-contrast MRI to improve precision of velocity field measurement. Magn Reson Med 2016;75(5):1909-1919.

85. Stemerman DH, Krinsky GA, Lee VS, Johnson G, Yang BM, Rofsky NM. Thoracic aorta: Rapid black-blood MRI with half-Fourier rapid acquisition with relaxation enhancement with or without electrocardiographic triggering. Radiology 1999;213(1):185-191.

86. Song HK, Wright AC, Wolf RL, Wehrli FW. Multislice double inversion pulse sequence for efficient black-blood MRI. Magn Reson Med 2002; 47(3):616-620.

87. Matsumoto K, Yokota H, Mukai H, et al. Coronary vessel wall visualization via three-dimensional turbo spin-echo black blood imaging in Kawasaki disease. Magn Reson Imaging 2019;62:159-166.

88. Swift AJ, Rajaram S, Marshall H, et al. Black blood MRI has diagnostic and prognostic value in the assessment of patients with pulmonary hypertension. Eur Radiol 2012;22(3):695-702.

89. Aghayev A, Rybicki FJ. State-of-the-art magnetic resonance imaging in vascular thoracic outlet syndrome. Magn Reson Imaging Clin N Am 2015;23(2):309-320.

90. Raptis CA, Sridhar S, Thompson RW, Fowler KJ, Bhalla S. Imaging of the patient with thoracic outlet syndrome. Radiographics 2016;36(4): 984-1000.

91. Hom JJ, Ordovas K, Reddy GP. Velocity-encoded cine MR imaging in aortic coarctation: Functional assessment of hemodynamic events. Radiographics 2008;28(2):407-416.